New York University
A private university in the public service

Neuromagnetism Laboratory
Departments of Physics and Psychology
and Center for Neural Science

ANNUAL TECHNICAL REPORT

Cognition and the Brain

15 February 1990 – 14 February 1991

Lloyd Kaufman and Samuel J. Williamson
Principal Investigators

New York University

Prepared for:

Dr. A.R. Fregly
Directorate of Life Sciences
Air Force Office of Scientific Research
Bolling AFB, DC 20332

Approved by:

Lloyd Kaufman

Samuel J. Williamson

Unclassified
SECURITY CLASSIFICATION OF THIS PAGE

REPORT DOCUMENTATION PAGE

1a. REPORT SECURITY CLASSIFICATION Unclassified	1b. RESTRICTIVE MARKINGS
2a. SECURITY CLASSIFICATION AUTHORITY	3 DISTRIBUTION / AVAILABILITY OF REPORT Approved for public release; distribution unlimited.
2b. DECLASSIFICATION / DOWNGRADING SCHEDULE	
4. PERFORMING ORGANIZATION REPORT NUMBER(S)	5. MONITORING ORGANIZATION REPORT NUMBER(S)
6a. NAME OF PERFORMING ORGANIZATION New York University 6b OFFICE SYMBOL *(If applicable)*	7a. NAME OF MONITORING ORGANIZATION Air Force Office of Scientific Research
6c. ADDRESS *(City, State, and ZIP Code)* Department of Physics and Psychology 4 Washington Place New York, NY 10003	7b. ADDRESS *(City, State, and ZIP Code)* Building 410 Bolling AFB, DC 20332-6558
8a. NAME OF FUNDING / SPONSORING ORGANIZATION AFOSR 8b OFFICE SYMBOL *(If applicable)* NL	9 PROCUREMENT INSTRUMENT IDENTIFICATION NUMBER AFOSR-90-0221
8c. ADDRESS *(City, State, and ZIP Code)* Building 410 Bolling AFB, DC 20332-6558	10 SOURCE OF FUNDING NUMBERS PROGRAM ELEMENT NO: 61102F PROJECT NO: 2313 TASK NO: A4 WORK UNIT ACCESSION NO:
11 TITLE *(Include Security Classification)* Cognition and the Brain	
12. PERSONAL AUTHOR(S) Lloyd Kaufman and Samuel J. Williamson	
13a. TYPE OF REPORT Annual 13b. TIME COVERED FROM 900215 TO 910214	14. DATE OF REPORT *(Year, Month, Day)* 910510 15 PAGE COUNT 61
16 SUPPLEMENTARY NOTATION	

17 COSATI CODES			18 SUBJECT TERMS *(Continue on reverse if necessary and identify by block number)*
FIELD	GROUP	SUB-GROUP	Cognition, spontaneous brain activity, alpha rhythm, cortical activity, magnetic source image, magnetoencephalography, sensory memory

19 ABSTRACT *(Continue on reverse if necessary and identify by block number)*

Using an array of 14 superconducting magnetic field sensors we succeeded in establishing the locations of neuronal activity that produce the dominant alpha rhythm recorded in the electroencephalogram and magnetoencephalogram. Of particular interest is our observation that spontaneous alpha activity is suppressed over the visual area when a person is engaged in mental imagery, and over other functional areas when appropriate cognitive tasks are performed. Computer simulations of the changes in patterns of alpha field power reveal how the power map is related to the underlying cortical topography when suppression occurs. In studies of sensory evoked cortical activity, an analysis of published current source density measurements on animals provides information from which we obtain the first realistic measure for the spatial extent of cortical activity in human cortex when responding to sensory stimuli. Measurements with a 5-sensor system for chrominance and luminance stimuli shows that the sites of response in visual cortex coincide. The separation of color information processing apparently takes place at a later stage, if at all. Responses in human auditory cortex to appropriate sound stimuli reveal activity not previously identified, which has characteristics that suggest it is related to sensory memory functions.

20 DISTRIBUTION / AVAILABILITY OF ABSTRACT ☐ UNCLASSIFIED/UNLIMITED ☐ SAME AS RPT ☐ DTIC USERS	21 ABSTRACT SECURITY CLASSIFICATION Unclassified
22a NAME OF RESPONSIBLE INDIVIDUAL Dr. Alfred Fregly	22b TELEPHONE *(Include Area Code)* 202/767-5024 22c OFFICE SYMBOL NL

DD FORM 1473, 84 MAR 83 APR edition may be used until exhausted
All other editions are obsolete

SECURITY CLASSIFICATION OF THIS PAGE
Unclassified

Contents

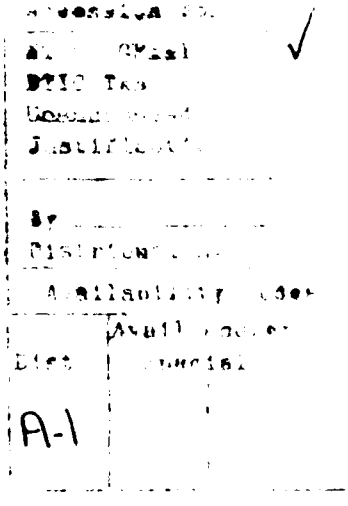

1 Introduction

This report, which is submitted in accord with the requirements of Contract No. AFOSR-90-0221 between AFOSR and New York University, describes the scientific progress made in the second year of support, from 15 February 1990 to 14 February 1991. The focus of this series of studies is to exploit certain advantages in the method of magnetic source imaging (MSI) to improve our understanding of cognitive functions of the human brain.

During the first year of this grant, we showed how magnetic measurements of the spontaneous activity of the human brain can discriminate between neuronal activity that is related to different cognitive functions. We found that the spatial patterns of suppression of activity within the alpha bandwidth (8 - 13 Hz) distinguishes between events related to mental imagery [44] and those related to silent speech [41]. Indeed, the pattern of suppression was localized over the respective cortical functional areas.

When a word is shown on a screen and the subject was instructed to find an image for the object it represents, suppression promptly commences over the occipital and parietal areas and is maintained for well beyond 1 s, until about the time the subject indicates by pressing a reaction time button that he has found an image. In these measurements, the level of alpha power from one moment to the next was obtained by averaging the variance of the signal across 30 epochs, using the onset of presentation of the word as the time reference. In contrast with this result, when the subject was instructed to find a rhyme to the word, suppression over the occipital area is maintained for a much shorter time, lasting for about 500 ms. Of particular note is the appearance of suppression over the temporal area for this task. Moreover, the temporal suppression begins after a delay of about 100 ms following the onset of presentation. This temporal suppression is maintained for well over 1 s until about the time the reaction time button is pressed, indicating that the subject has found a rhyme. The difference between the timing and patterns of suppression cannot be accounted for by differences in task difficulty, because reaction times for the two tasks were about the same. Therefore, the onset of suppression is not caused by a generalized attentional effect, but relates to the specific congitive task.

Pfurtscheller et al. [82] first called attention to the spatially selective aspect of alpha suppression, by measuring the electroencephalogram (EEG) with an array of electrodes placed across the scalp. However, in his work it was necessary to limit the measuring bandwidth to about 1 Hz to detect the spatial variation by comparing the patterns for "low-band" alpha (about 9-10 Hz) and "high-band" alpha (about 11-12 Hz). High-band alpha was found suppressed over the occipital area whereas low-band alpha was suppressed over centeral areas, when a subject was engaged in a visual motor task. Unfortunately, this narrow band recording severely limits the response time for measurements, so that sharply defined onset and release of suppresion were not observed. By contrast, neuromagnetic measurements provide a more sharply confined pattern of activity across the scalp, so that different behavior over temporal and occipital areas could be detected easily with wideband recording, which extend over the complete alpha bandwidth. In this way, sharp onsets of suppression can be observed at appropriate positions.

Our findings support the notion that spontaneous rhythms are produced by many areas of cerebral cortex. This rhythmic activity is locally suppressed when a particular area becomes engaged in sensory or cognitive functions. Therefore, by monitoring the pattern

of spontaneous activity across the scalp it may well be possible to follow the sequence of activity in a particular individual and to determine the particular strategies that the person relies on to carry out specific functions.

During the past year we developed two complementary approaches to elucidate the nature of this spontaneous activity. One is based on the approach that seeks to indentify the location of the underlying neuronal activity moment by moment. The other focuses on the time average features of activity, to characterize the pattern of average power across the scalp and how it relates to underlying cortical topography. Both studies seek to improve our understanding of the nature of suppression phenomena, so that this measure of cognitive function can be extended to characterize other cortical areas and deal with single events. By introducing models for the underlying neuronal activity we seek to provide a more quantitative measure of the level of cognitive activity that is recruited during higher levels of brain processing.

A third project completed in the early part of last year turned out to have relevance to our studies of spontaneous rhythms. Several years ago we became curious as to why the cortical response level (characterized neuromagnetically by the current dipole moment) is relatively insensitive to stimulus strength, unless the stimulus is very close to threshold. In other words, response strength is not an accurate gauge of stimulus strength except for very weak stimuli. In fact, Pantev et al. [80] reported that the N100 component of the auditory evoked response has an *amplitopic* representation across cortex. This means that stimuli of differing strengths evoke cortical activity at different locations, with the current dipole moment being insensitive to strength. One of our graduate students, Zhonglin Lü, took on the challenge of inspecting published electrophysiological data on animals to determine whether there is a basis in that literature for what is seen by MSI. This was successful, as he found that for cat visual cortex and monkey somatosensory cortex, with a variety of stimuli, the current dipole moment under each square centimeter of active cortex is approximately the same value. It is 50 pA·m for each mm^2, to within a factor of two for all the reliable data considered. This means that once the current dipole moment for activity in sensory cortex of human is deduced magnetically, it is possible to use this conversion factor to deduce the total cortical area that contributes. For commonly found dipole moments, ranging from 2 to 20 nA·m, the corresponding cortical areas range from 40 to 400 mm^2. The smallest limit is larger than a macrocolumn and the largest is a good fraction of a cortical representation area. When this factor is applied to the strength of alpha rhythm, as represented by the current dipole moment of a typical alphon, the active cortical area is typical several square centimeters. There is some justification for this application, since the transcortical voltages revealed by the measurements of Lopes da Silva and Storm van Leeuwen [60] on dog during well-developed alpha rhythm are comparable to those seen during peak activity of late components of sensory evoked responses.

A fourth project was also completed last year. We investigated the possibility that chrominance information in a visual stimulus is processed in some stages in visual cortex by a population of neurons in visual cortex that is spatially distinct from neurons processing luminance information. If so, neuromagnetic techniques could be applied to study separate aspects of chrominance and luminance processing. This was carried out first at NYU with our 5-sensor probe as part of Gladys Klemic's Masters Thesis in Physics, and responses for well-controlled luminance and chrominance stimuli were obtained. Subsequently she par-

ticipated with the group in the Low Temperature Laboratory at the Helsinki University of Technology (HUT), under their sponsorship, and used their new 24-sensor probe. The collaborators at NYU were G. Klemic, L. Kaufman, J. Krauskopf, and S.J. Williamson, and the collaborators at HUT were S. Ahlfors, R.J. Ilmoniemi, O.V. Lounasmaa, and S.T. Lu. This study was motivated by previous clinical [5, 97], physiological [53][125], and psychophysical [48] studies which suggest that at certain stages chrominance and luminance information is processed by separate neuronal populations. Neuromagnetic responses to chrominance stimuli along the red-green axis and to luminance changes of an achromatic stimulus were compared for latencies up to 400 ms. Extensive measurements with a 5-channel axial and a 24-channel planar SQUID gradiometer found no significant spatial divergence. The latencies of chrominance responses were consistently longer than those for luminance responses over a wide range of stimulus levels. Only when the luminance was decreased to near threshold levels did the corresponding latency increase sufficiently to exceed that for the chrominance responses.

A remarkable finding emerged from a sixth study, which was carried out as a part of our investigation of short-term memory. This was discovery of two temporal components of the auditory evoked response that are clearly revealed when the interstimulus interval (ISI) is sufficiently iong. While is it likely that prior EEG studies had identified signals from these sources, the sensitivity of their strength to ISI and determination of their exact locations in the brain were first achieved in this study. The timing of this activity indicates that several major functions fo auditory cortex are carried out in parallel, with both primary and secondary cortex participating. Such feedback connections had recently been found via electrophysiological studies of visual cortex in animals, and this present finding may well be the first evidence for such an organization in the auditory system.

The following sections give detailed accounts of the accomplishments in the six areas mentioned in the preceding summary.

2 Localization of Dominant Alpha Rhythm Sources

Many areas of human cerebral cortex support spontaneous rhythmic activity. Many of these areas can be identified by magnetic measurements, and it is of interest to do so. The principal motivation for this is our finding that these rhythms are selectively suppressed when specific areas of cortex engage in cognitive functions. For this reason, we have investigated the properties of the best-know spontaneous rhythm – alpha rhythm.

Alpha rhythm was the first electrical signal of the human brain to be recorded noninvasively (Berger, 1930) [4]. The cortical origin of this signal is well established through studies of the transcortical voltage profile in the visual cortex of dog [60]. Alpha rhythm is known to involve thalamic projections to cortex [1] but the precise relationship is yet to be established. Direct evidence for this connection is the appreciable coherence observed between cortical potentials in pulvinar and visual cortex [58] [59]. However, these same studies reveal that the coherence between two regions of cortex separated by as much as 6 mm is much greater than the coherence with activity in the pulvinar. This suggests that intracortical interactions play a more important role in the spread of activity across cortex.

We have coined the name *alphon* to denote the cortical excitation that gives rise to an alpha spindle originating within the parieto-occipital sulcus [121]. These are the strongest

sources of signals that can be detected magnetically and electrically from normal subjects. During the past year we have extended our previous work that seeks to define the cortical locations of this activity. We have previously established that the neuronal sources of individual spindles are different geometrically [35]. That is, alphons differ from each other in location, extent, shape of active cortical area, or orientation of net intracellular current. Only about 2% of the alphons cannot be distinguished from another one. This feature was established without recourse to a specific model for the alphon, such as a current dipole model. Since 14 sensors were employed in the measurements, each spindle could be represented by a 14-dimensional vector in this sensor space. If two vectors are significantly different in orientation, in comparison with the noise level, their field patterns are distinctly different. Correspondingly, the underlying neuronal sources (alphons) are physically distinguishable. In this way we established the fact that the parade of spindles seen in the MEG and EEG arise from different spatial configurations of neuronal activity.

With improved analysis procedures we were able to show during the past year that individual oscillations produced by an alphon arise from neuronal activity that exhibits a remarkable spatial stability. The center of activity giving rise to successive oscillations is found to shift by less than a couple of millimeters, suggesting that a spindle is not a happenstance arising from constructive interference of field patterns of many separately oscillating regions of cortex. Rather, it represents a coherent oscillation of a wide area of cortex, which can be as large as several square centimeters. This estimate arises from our study of current source-density measurements to be mentioned later.

Measurements were made with a pair of 7-sensor magnetic probes located in the Center for Neuromagnetism at the NYU Medical Center. Simultaneous measurements are essential to determine the field pattern of spontaneous activity moment by moment, for it is a changing pattern. They were positioned with probes over the left and right parieto-occipital areas to record simultaneously where magnetic field emerges and enters the head during alpha activity. Typical signals within the alpha bandwidth are shown as a parade of spindles in Fig. 1. This particular example was obtained by Ilmoniemi et al. [35].

There are clear differences in the relative amplitudes across sensors for successive spindles, indicating they originate from differing neuronal populations. The sensitivity in discriminating between sources is determined by the noise level, which in this case is determined by other ongoing signals of the brain. Typically only 2 of 30 spindles had directions that were indistinguishable for their signal vectors. Therefore, human alpha rhythm arises from a wide variety of sources, distinguishable by differences in their geometry and/or location. A similar approach for discriminating among event-related potential distributions had been suggested by McCarthy and Wood [66]. A more detailed study permitted us to address the question as to exactly where these alpha spindles originate. Earlier neuromagnetic attempts [115] to locate the sources of individual spindles by invoking a current dipole model for each one suffered from poor resolution, because only a 4-sensor probe was available. A minimum of 5 measurements are required, because a current dipole determined magnetically is characterized by 5 parameters (3 for position, 1 for the orientation of the moment in the plane tangent to the overlying scalp, and 1 for the magnitude of the moment). By assuming that the current dipole is oriented parallel to the longitudinal fissure, Vvedensky et al. arrived at the conclusion that alpha sources are distributed within a wide region of the occipital lobe.

In our study a current dipole model for each spindle was applied to recordings made with

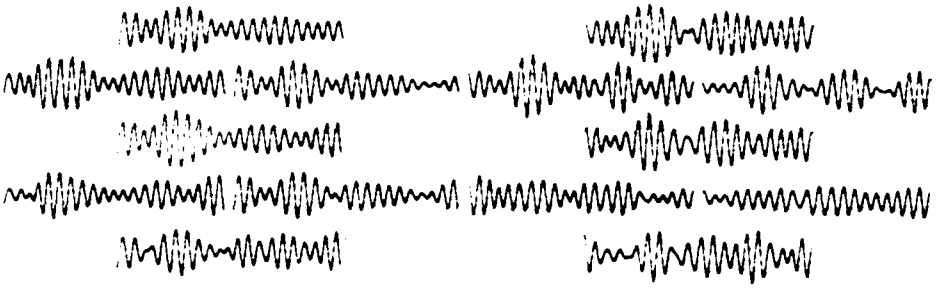

Figure 1: Successive spindles recorded within a time series of 4 s duration within the bandwidth 8-13 Hz from two 7-sensor probes. The approximate position of individual sensors within each probe are shown by the placement of the recordings. Probes are positioned 6 cm above the inion and 4 cm to either side of the midline.

the 14-sensor array as described earlier, but with the probes at different relative positions, including having one farther above the inion than the other to detect dipoles that are tipped out of the sagittal plane. In fact, the deduced directions were always within about 30 deg from that plane. To achieve maximum accuracy in locating the sources, individual sensors were calibrated with an accuracy of better than 2%. This was necessary, because the field extrema were so broad that differences in field strengths at the sensors were often only 10%-30% of the total field. Therefore, high absolute accuracy in calibration was essential to achieve decent measures of these field differences across sensors. Similarly, to improve the signal-to-noise ratio, a best estimate for the amplitude of a spindle detected by a given sensor was obtained from the sum of the covariances between that sensor's signal and all the other sensors' signals. This was computed over the time span for which spindle signals exceeded minimal strengths preselected by the experimenter and the period of the oscillation was stable to better than 3%.

The procedure was successful in localizing spindle sources with an accuracy that is typically ± 0.8 cm in depth beneath the scalp and ± 1.3 cm for distance above the inion (95% confidence). Examples are shown in Fig. 2a as reported by Williamson et al. [120]. Most sources are localized to parieto-occipital fissure, with a few also occurring in the calcarine fissure. Most puzzling is the lack of sources in the portion of visual cortex forming the walls of the longitudinal fissure. The positions illustrated are obtained from spindles that produce a field extremum under at least one of the probes. Greater accuracy is obtained if a field extremum lies under each probe [12], but there were few spindles found to be positioned and oriented in such a way as to do this for the 14-sensor array in a fixed location. Even if data are fit when neither extremum lies under a probe the center of the distribution coincides with that of Fig. 2a, although the scatter in positions is 30% greater. Another important result from these studies is the first measurement for the distribution of current dipole moments. The distribution of source strengths clusters around an average value of 40 nanoampere-meter (40 nA·m), with the width at half maximum being a comparable value

a

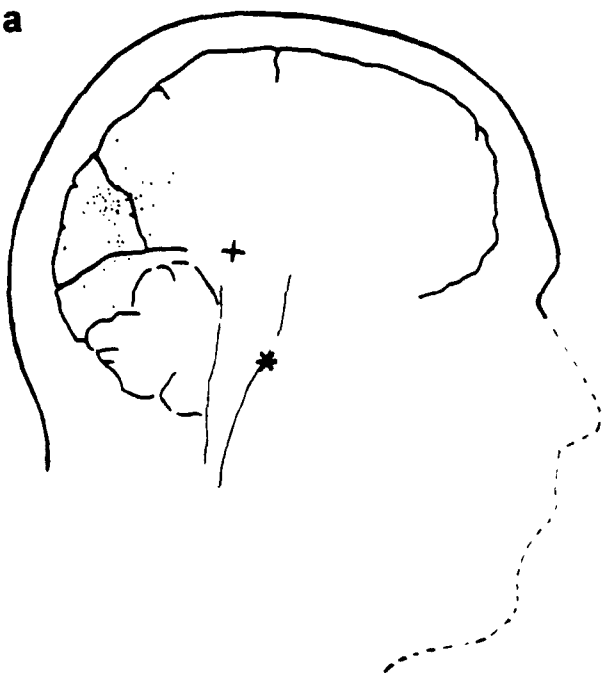

b

Peak No.	Anterior x (cm)	Leftward y (cm)	Upward z (cm)
1	- 4.86	0.01	2.12
2	- 5.54	- 0.37	7.31
3	- 6.07	- 0.64	7.49
4	- 6.28	- 0.72	7.62
5	- 5.91	- 0.34	7.56
6	- 5.38	0.06	7.06
7	- 5.28	- 0.41	7.16
8	- 4.79	0.18	5.67
9	- 5.91	- 0.75	6.73
10	- 5.92	- 0.32	6.19
11	- 5.73	- 0.37	6.36
12	- 5.79	- 0.40	6.91
13	- 5.69	- 0.33	6.42
14	- 6.36	- 0.79	7.74
15	- 6.09	- 0.58	7.10
16	- 6.72	- 0.78	8.51
17	- 6.45	- 0.84	8.15

Figure 2: (a) Positions of alpha spindle sources shown in relationship to parieto-occipital fissure and calcarine fissure, as obtained from MRI scans of the subject. (b) Sequence of positions for individual successive signal peaks, expressed in the head-based coordinate system, whose origin is midway between the left and right periauricular points.

[121].

This study demonstrates that is it feasible to locate neuronal sources of individual spindles. At the level of accuracy achieved in these first measurements, the results are anatomically reasonable. Moreover, a remarkable finding emerged from the analysis: no spindles were found within the longitudinal fissure, and comparatively few were identified with the calcarine fissure. Primary visual cortex appears to produce a lower level of alpha rhythm than the other visual areas.

Recently we have carried out dipole fits to individual peaks of a series of spindles (Z. Lü, J.Z. Wang and S.J. Williamson, in preparation). Representative results are shown in Fig. 2b for three successive spindles. Peak 1 is rather weak, but peaks 2-5 correspond to the stronger central region of the first spindle. These data show that the shift in location along any axis with respect to the average position is only a few millimeters. Similarly, peaks 9-13 reveal another series of stable positions and correspond to the strong interval of the second spindle. Finally, peaks 14-17 of the third spindle represent another stable sequence. These data indicate that for reasonably strong spindles the peak-to-peak center of neuronal activity can be followed without need to average across the duration of a spindle to determine locations with acceptable precision. The data provide a series of time segments within which the neuronal source exhibits a stable configuration for a few oscillations (our technical definition for a "spindle") but then switches to a different configuration. These

moments of source stability may very well correspond to the time segments described by Lehmann [52] as "brain states" where the power distribution in the alpha band across 19 EEG electrodes on the human scalp remains stable for a fraction of a second. His data show abrupt shifts in the global power pattern (and therefore the corresponding sources) from one time segment to the next.

A chi-square cost function was used in fitting the dipoles to the field data, so we obtained a measure of the significance of the fit by using the observed signals with subject's eyes open as a measure of the noise. The probability of attaining the observed minimum value of chi-square was sufficiently high as to admit the current dipole as a reasonable model. However, there were other time segments of successive peaks where the source location is quite stable but where the probability is sufficiently low to suggest that an extensive source model would be more appropriate.

That some spindles may arise from extensive sources is supported by a recent analysis by Lü and Williamson [61] of published current source-density studies of sensory evoked activity in cat visual cortex and monkey somatosensory cortex. This analysis shows that the transcortical current dipole moment associated with intracellular currents at moments of peak activity for long latency components is about 50 pA·m per mm^2 of cortical surface. This number holds to within a factor of 2 for a variety of stimuli. Lü and Williamson (unpublished) have recently analyzed the potential profiles recorded during alpha activity in dog visual cortex [60] and find that the peak current dipole moment per mm^2 of surface is comparable to the value cited above for sensory evoked activity. Therefore, the value of 40 pA·m for the current dipole moment associated with a typical, strong alpha spindle may also be applied, to first approximateion, for alpha rhythm. The corresponding area of activity associated with a strong alpha spindle is therefore about 800 mm^2. If this represents a continguous area, it would be embraced by a boundary of about 3 cm×3 cm in linear dimensions. This is quite remarkable, since it represents the major portion of the posterior bank of the parieto-occipital fissure in either the left or right hemisphere. This suggests that the spatial coherence length for human alpha activity can be of comparable length. This model supports the much earlier findings by Lopes da Silva and Storm van Leeuven [60] of long-range coherence in cortical rhythms. However, they report a much shorter coherence range of about 6 cm deduced from multi-electrode studies in dog. The mediator of coherence may well be laminar-parallel intracortical fibers which extend 6 - 8 mm [59], together with pyramidal collateral spread modules which extend over about 3 mm [15].

3 Influence of Cortical Topology on Neuromagnetic Field Patterns

There is considerable evidence that magnetic source images can be obtained with an accuracy of better than 3 mm for neuronal activty of normal levels in sensory cortex. This procedure relies on modeling the neuronal source as a single current dipole, a point source having a direction and strength. However, this approximation has important limitations when modeling spontaneous activity, because there is growing evidence that widespread areas of the brain support such activity. To model spontaneous activity it is necessary to consider effects of convoluted source configurations, representing the topography of cortex.

This is of particular interest in light of our recent cognitive investigations that depend on the fact that spontaneous activity is locally suppressed when cerebral cortex becomes engaged. Distributed neuronal activity across such convoluted terrain can result in time-varying field patterns that may be intepreted incorrectly as being due to rotating and moving patterns of neuronal currents within the cortex. Thus, changes in field patterns, (and patterns of potentials too) can arise over time because of changes in the distribution of activity within a population of neurons, and this will also depend upon the geometry of the source configuration. These and related phenomena have profound implications for interpreting changes in brain activity conventionally attributed to *synchronization* and *desynchronization*, states of activity that are often presumed to underly alpha production and its blockage. It also has implications for understanding other phenomena observable in the now widely used topographic displays of the EEG [51], [23] [22], as well as the MEG, although topographic displays of the real-time MEG have yet to be employed.

Let us now consider a single current dipole. By computer it is straightforward to find an exact numerical solution for its field at the surface of a sphere.[1] In this example (Fig. 3a) the dipole is 6 cm away from the center of a 10 cm radius sphere. The values of the field, which are "measured" at 841 points on the surface of the sphere are projected onto a plane. The plane itself is placed at right angles to the radius between the sphere's center and the dipole and is tangential to the sphere itself. Fig. 3b shows the actual isofield contour map. The (0,0) coordinate is directly over the dipole, and the field extrema are the centers of the innermost isofield contours at the left and right. While the relative field strengths of the contours is fixed by the geometry, the overall strength is arbitrary and is proporational to the current dipole moment. Following the prescription of Williamson and Kaufman [118], we can easily tell that this dipole (of strength $|\vec{Q}|$) is located 4 cm beneath the surface and lies exactly between the field extrema.

In practice one cannot measure the field at a very large number of positions simultaneously. Although magnetic field measuring systems composed of 37 independent sensors have recently become available, they are not yet widely used. It is more common for investigators to make large numbers of sequential measurements, generally using systems consisting of a few sensors. In fact, the widespread use of sequential measurements rather than many simultaneous measurements may well have led to the emphasis on single current dipole models, as it is not possible to determine the ever-changing field pattern asociated with the spontaneous activity of the brain from sequential measurements.

3.1 Cruciform Source Configuration

In attempting to explore how the detailed shape of the brain influences the field pattern generated by extended sources, we employed a source configuration based on the cruciform model of the visual cortex (Fig 4a). With a dipole for every square millimeter of surface within the fissures and sulci of the model, we have a complex geometry containing 1386

[1] More realistic models of the head can be used in place of a sphere [21] [26] [67]. However, the sphere of uniform conductivity fitted to the inner contours of the skull in the region above the source is adequate in many - though not all - areas of the human brain for magnetic localization of current dipole sources with an accuracy of better than 3 mm.

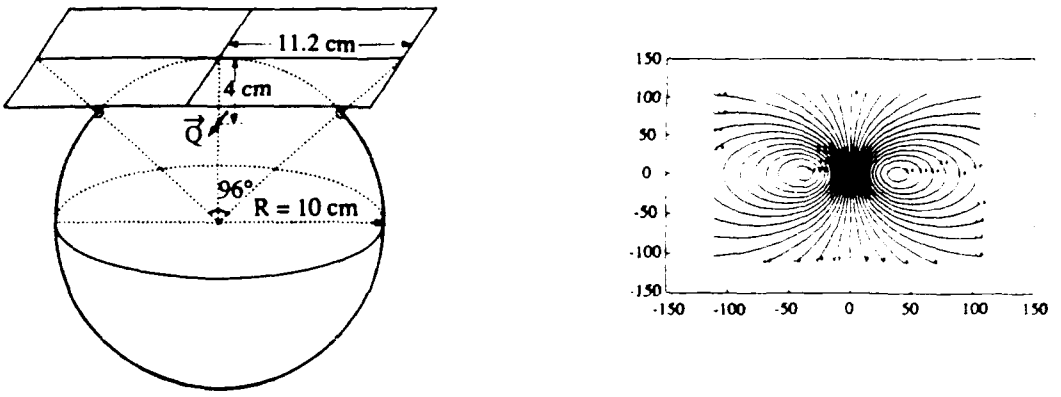

(a) (b)

Figure 3: (a) Spherical representation of the head with a current dipole $\vec{Q}$ representing an area of cortical acitivty located 4 cm beneath the scalp. Above it is a plane onto which the field pattern across the scalp is projected for display. (b) Isofield contours for the field pattern.

dipoles. Each dipole may be thought of as a column of neurons oriented normal to the surface of the cortex. The opposed walls of the simulated longitudinal and calcarine fissures are separated from each other by 4 mm. All fissures are 2 cm deep and, normal to the radius passing through the center of the structure, 1 cm wide and 1 cm high. As shown in Fig 4b, the cortical surface farthest from the center of the sphere is 3 cm away from the sphere's surface. The model cortex extends 2 cm deep, so its innermost elements are 5 cm from the center of the 10 cm radius sphere.

3.1.1 Computing the Field

The maximum field strength at the scalp produced by a current dipole varies inversely with the square of its distance from the scalp. Within a homogeneous medium, the field produced by a current dipole is given by the following equation:

$$\vec{B}(\vec{r}) = \frac{\mu_o}{4\pi} \frac{\vec{Q} \times (\vec{r} - \vec{r_o})}{|\vec{r} - \vec{r_o}|^3}$$

Where $\vec{B}(\vec{r})$ is the field at a point $\vec{r}$ in space, $\vec{r_o}$ is the vector from the center of the sphere to the dipole, $\vec{Q}$ is the current dipole moment, and μ_o is the permeability of free space. Since we are interested in only the radial field external to the sphere, this normal component of $\vec{B}$ is simply the dot product (scalar product):

$$B_n = \vec{B} \cdot \frac{\vec{r}}{|\vec{r}|}.$$

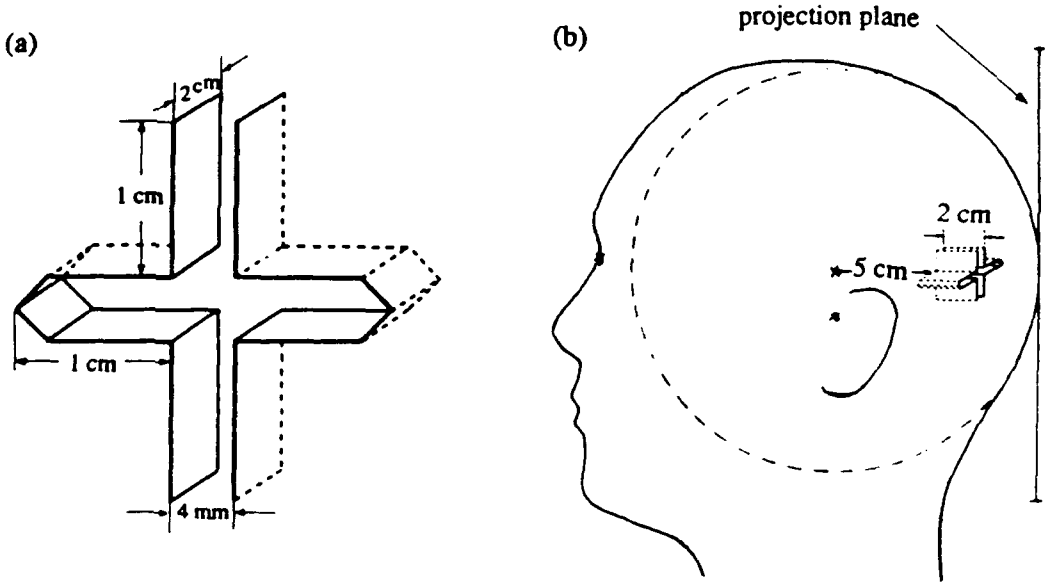

Figure 4: (a) Cruciform model of visual cortex, with the longitudinal fissure forming the arm that divides left and right sides. The other arm is formed by the calcarine fissure, whose floor and ceiling lie approximately in the transverse plane. (b) Placement of the cruciform within the head, for purposes of the model.

By superposition (c.f. Jackson [36]), we can solve the field of each of the 1386 sources separately and add the resulting vectors computed at $29 \times 29 = 841$ points on the sphere's surface. We then calculate the radial component (B_n) of each field vector (which is the physical quantity measured in MEG experiments) at positions on a spherical surface. These values are then displayed by the use of isofield contours, which characterize the pattern of the radial field strength projected onto a plane placed tangential to the scalp. The sides of this plane are 22.4×22.4 cm, as illustrated in Fig. 3a. The center of this projection on the place is directly over the radius of the sphere passing through the geometrical center of the cruciform model.

3.1.2 Simulating an Evoked Response

To test the implmentation of the model described above, we simulated an evoked response due to the activation of a portion of its dipole population. To conduct this test it was necessary that we be even more specific about the assumptions related to the nature of the activity underlying *evoked responses*. Therefore, we asssumed that all the dipoles comprising a 1 cm deep portion of one quadrant (the shaded areas of Fig. 5) were oriented in the same direction. In separate simulations two different 1-cm deep portions of one quadrant were used. One of these regions was the outer half of the quadrant (Fig. 5a), which was therefore bounded by an outer border 3 cm from the surface and an inner border 4 cm from the surface of the sphere. The other portion (Fig. 5b) was delimited by borders 4 cm and 5 cm deep. The directions for all of the other dipoles in the model were randomized. The dipole moments of both the synchronized (same direction) dipoles in the small portion, and of the larger asynchronous (random directions) remainder of the structure were randomized, and, on average, the level of activity per unit area of the two regions was about the same.

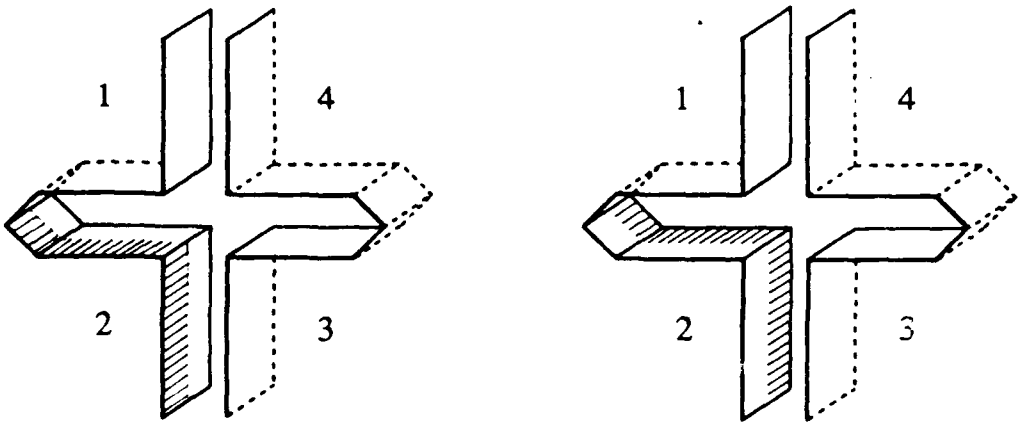

(a) (b)

Figure 5: (a) Synchronized neuronal activity (shaded area) spread across the lower left quadrant of visual cortex, portrayed on the cruciform model. (b) Deep synchronized activity of the same area.

This simulates a situation where neurons of an array of dipoles within a portion of sensory cortex are made to respond synchronously to a stimulus (but not increase in level of activity after stimulation as it might be presumed to do in the case of evoked neuronal activity), while the larger unaffected portion continues to exhibit random asynchronous activity, but at the same average level per unit area. To mimic changes in the field pattern with time, the orientations of these dipoles (inward toward the depth of the brain or outward toward the surface of cortex) and moments were changed. One hundred different patterns were generated, and the average of all patterns was computed. Thus, we were able to test the model and determine if it is possible to accurately locate the center-of-gravity of the array of synchronously active dipoles regardless of the effects of dipoles comprising its surroundings.

Figure 6 contains samples of "instantaneous" field patterns that represent the field a an instant of time, as well as two average field patterns. The instantaneous patterns ar· asymmetrical (could be described by a superposition of multipolar sources) and may be quite different from each other. That is, their field extrema are at different places, depending upon the set of random numbers describing the dipole moments. This difference is especially pronounced between the two left-hand patterns of the lower row in the figure, and they illustrate the claim made in the introduction that field patterns obtained at any "instant of time" can differ from those obtained at other instants of time. However, as a result of the averaging processs, the features that change from one distribution of dipole moments to another tend to be self-cancelling, while invariant features not visible in the individual plots are relatively enhanced. For this reason the two averaged isofield contour plots in Fig. 6 are apparently dipolar in character. Note that the extrema obtained with the deeper synchronized portion are clearly farther apart than are those obtained with the more shallow synchronized portion. Also note that the point lying midway between the two extrrema in each of the averaged plots is offset from the center to a position directly above the center of the synchronized quadrant.

If the invariant features are attributable to the activity of a synchronized subset of the dipoles, then the depth of an equivalent current dipole best representing that subset should

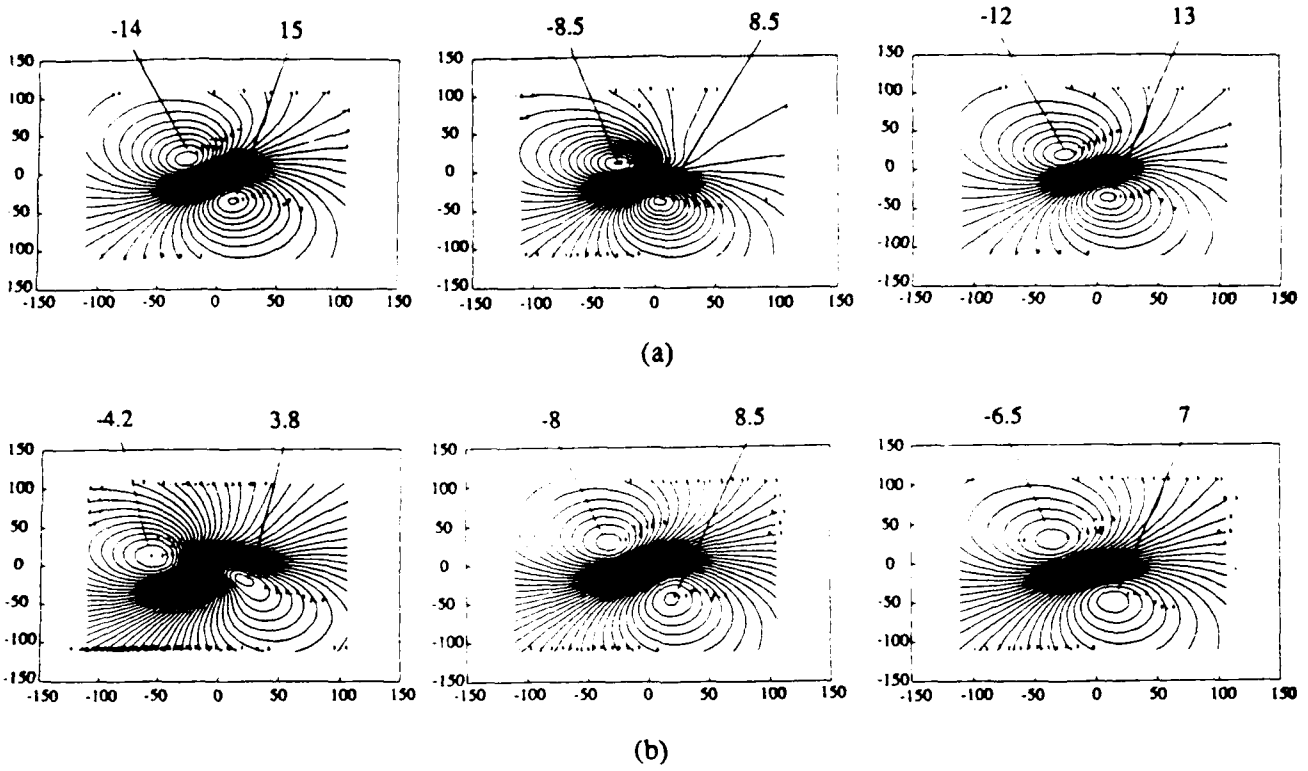

Figure 6: (a) The two isofield contours on the left are samples of the instantaneous field patterns obtained when a shallow region of lower left quadrant of the cruciform structure contains synchronized dipoles. The plot on the right is the average of 100 such samples, and it exhibits a dipolar pattern centered directly over the shallow shaded region and slightly displaced from the center of the cruciform structure. (b) The two patterns on the left of the lower row show instantaneous fields generated when a deeper region of the lower left quadrant contains synchronized dipoles. The plot on the right is the average of 100 samples. Note the greater separation between the field extrema of the average plot of this series. It corresponds to the greater depth of b relative to a.

be approximated by the geometric mean of the depths of the innermost and outermost boundaries of the region it occupies. This follows from the fact that field strength at individual extrema varies inversely with the square of the distance to its source, so the fields of dipoles near the outermost boundary of the region should be more strongly represented in the field at the surface than those of dipoles near the deepest boundary.

In this numerical simulation small deviations from this geometrical mean are to be expected because it is an approximation, and because of the presence of sampling imbalances in the sets of random numbers. These geometric means are 3.45 cm for the shallow (Fig. 5a) and 4.47 cm for the deeper (Fig. 5b) synchronized portions of the cruciform structure. Calculating the depths of the equivalent current dipoles from the angular separations of the average extrema on the surface of the sphere gives values of 3.53 cm and 4.49 cm for these same two portions, respectively. similar values were obtained in replications of the simulation, but with two different quadrants of the model.

This example illustrates how the single equivalent dipole model may be used to determine

the location of the center-of-gravity of an extended set of dipoles, and this success sets the stage for consideration of more complicated dipole arrays.

3.2 Results

3.2.1 Synchronous versus Asynchronous Activity

As shown in the previous example, field patterns associated with random current dipole moments vary widely, depending upon the distribution of dipole moments within the array. In the face of such variability, it is difficult if not impossible to interpret any individual pattern as being due to activity within a particular structure. However, when a small region of synchronized activity is present, a stable pattern emerges after averaging, and this pattern is clearly related to the location and orientation of the underlying synchronized sources within the cruciform structure. This suggests that it is worthwhile to explore further the differences and similarities between effects of synchronous and asynchronous activity.

In many textbooks, synchronization is described as a basis for alpha activity and the slow EEG waves occuring during sleep, while desyncrhonizatin is presumed to be the proximate "cause" of alpha blockage and the relatively fast activity associated with arousal (cf. [107]). These same terms are widely used with the same sense in the literature (cf. Pfurtscheller and Aranabar [83], but see Hobson and Steriade [32] for cautionary language). To simulate synchronization in the context of the cruciform structure, all of the dipoles in its walls were oriented in the same direction, e.g., all were directed inward from the surface of the cortex (Fig. 7a). However, the magnitudes of these dipoles differed randomly from one position to the next, and the pattern of random values was changed to discover how different distributions of dipole magnitudes affect the field pattern outside the sphere.

It should be noted that the term *synchronization* need not imply that the directions of current flow is the same for *all* of the columns represented by the dipoles, as assumed here. Alternatively, synchronization of activity could be limited to one or more small cortical regions or patches, as in the example of the evoked response described above. Also, synchronization could mean that several patches, located at various distances from each other, are more or less loosely coupled to each other, and the level of correlation of activity between the patches could be related to the distance between them. Internally synchronized patches may oscillate independeltly of each other. In fact, Lopes da Silva and van Leeuven [60] demonstrated that alpha band activity across the surface of the dog's visual cortex exhibits coherence (synchronization) over distances no greater than 6 or so millimeters. Measurements on human subjects, described elsewhere in this report, indicate that coherence can extent for several centimeters for alpha activity within the parieto-occipital sulcus. However, the strong spindles that are associated with this activity have not been detected from visual cortex or other areas of the human brain. We may infer, therefore, that spontaneous rhythms that arise within the cruciform model or from these other areas of cortex are produced by cortical activity whose spatial coherence extends for only a few millimeters. Instead, the summed activity of a number of largely independent generators oscillating at frequencies within the alpha bandwidth may well produce what is often described as circulating and moving "coherent" patterns of alpha activity in the EEG. Because of this, we chose to use a model in which there is no synchronized activity outside the 1 mm area assigned to a given dipole to produce our asynchronous model. This mimics a situation in which 1 mm square

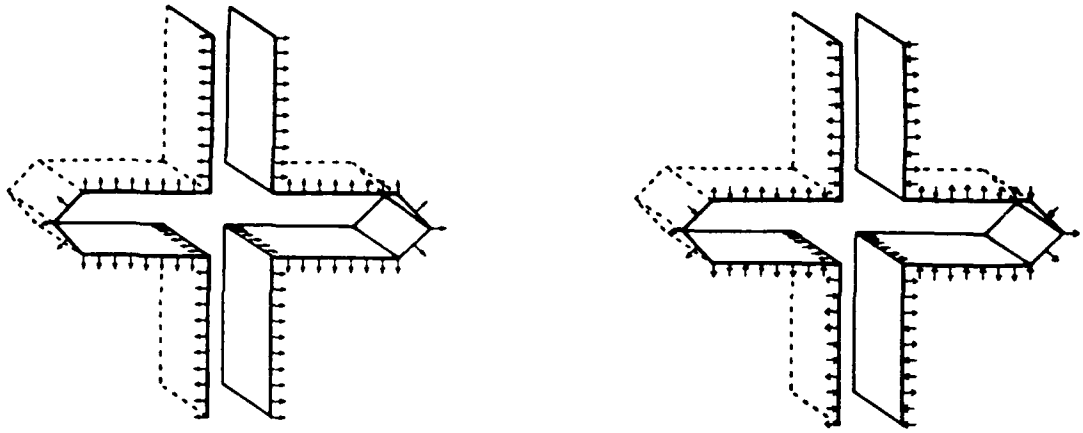

Figure 7: (a) Simulation of synchronization, here defined as having all dipoles aligned in the same directions relative to the cortical surface of the cruciform structure. Their magnitudes may be equal, or distributed randomly. The latter means that all dipole moments range from 0 to +1. (b) Simulation of asynchronization, which means that dipoles have random directions as well as magnitudes. Their moments range from −1 to +1.

areas of cortex oscillate at alpha (or other) frequencies independently of each other (Fig. 7b).

More concretely, we represent activity by selecting a random value from −1 to +1 to represent the net current of any of the 1386 small 1 mm×1 mm columns that form the mosaic of activity across cortex. The net external field resulting from the superposition of the fields associated with each of these sources is computed. To represent the state of the cortex at different times, the simulation was run a number of times applying different initial seeds to the random number generator. Each initial random seed is associated with a different list of random numbers, and the patterns were generated by assigning these numbers to the dipoles in the array, beginning at different places in the list. For each pattern, the average amount of activity in each wall of the cruciform model was approximately the same, thus enabling us to directly test the idea that differences in the statistics of the dipoles rather than their net energy will affect the distribution of the external fields. Figure 8a contains representative field patterns generated by the synchronized dipoles where only current magnitudes were randomized.

Despite obvious differences among the patterns they all seem to share some common features. Synchronization results in remarkably stable patterns regardless of changes in the moments of the dipoles. In fact, averaging across a large number of different patterns for each of three initial seed results in the generation of very similar multipolar patterns, where each of them contains four extrema.

This may be contrasted with the field patterns obtained using arrays of asynchronous dipoles, those generated by selecting a value of −1 to +1 to represent the current of any

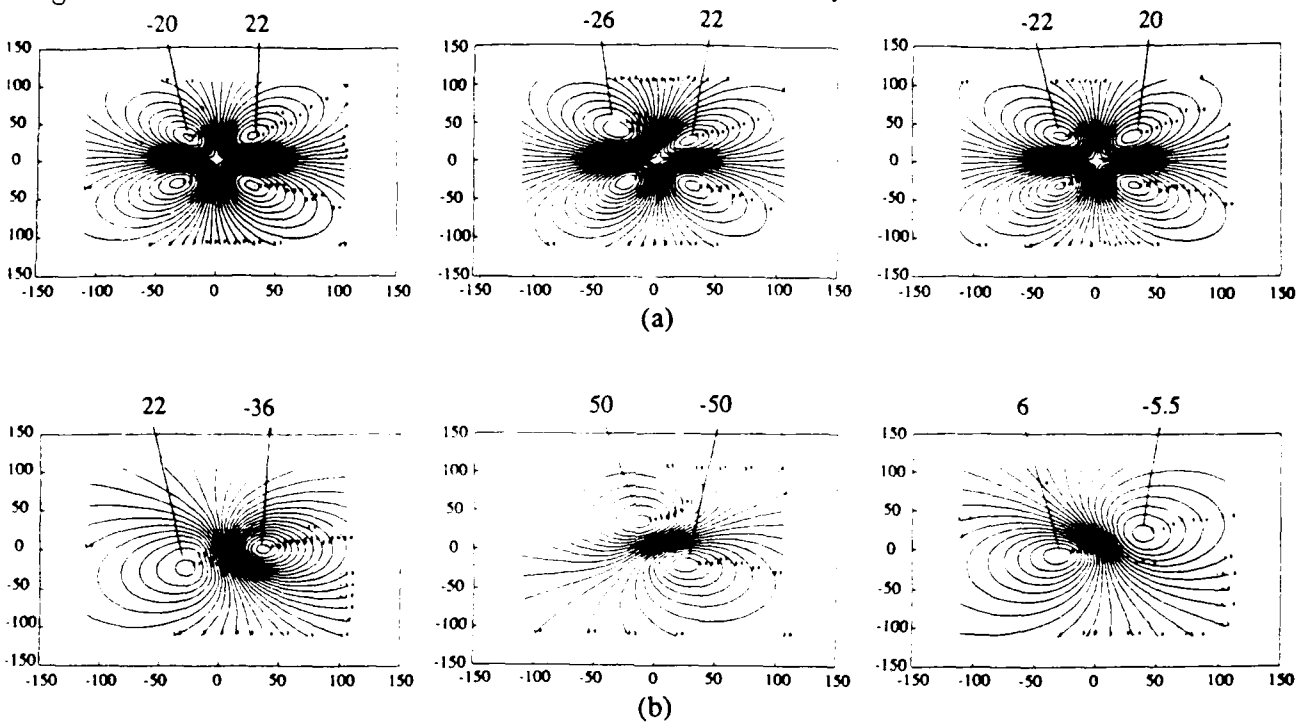

Figure 8: (a) The two left hand instantaneous field patterns are produced by synchronized dipoles with randomly different magnitudes. An average of 100 such patterns is shown at the right. Numerals above each pattern indicate the relative field values at the extrema. (b) The two instantaneous field patterns at the left are associated with asynchronous dipoles. Note the greater differences between them compared with the similarity illustrated in the first row for synchronized dipoles. Note also that the field strengths vary considerably. The average of 100 patterns on the right exhibits a much weaker pattern because of cancellation effects.

one of 1386 dipoles (Fig. 8b). The instantaneous patterns obtained for different random arrays are generally quite different from each other. Although the centers of these patterns are located more or less directly over the radius of the head passing through the center of the cruciform structure, the asymmetric extrema found in most patterns seem to rotate around that center. From one field pattern to another, extrema of opposite signs (emerging or reentering field) often appear at overlapping position in otherwise similar patterns. In fact, the extremely low field strength in the averaged patterns shown in Fig. 8b is due to the fact that fields of opposed sign tend to cancel each other in generating the average plot. These average field values are clearly weaker than those obtained with synchronized dipole arrays.

However, the differences between the average fields obtained with synchronous and asynchronous arrays do not demonstrate that desynchronization (shifting from synchrony to asynchrony) leads to weaker fields. Note in Fig. 8 that the peak values of the instantaneous fields associated with the synchronized array of dipoles have arbitrary values of 20 to -26 units of field, while those associated with the desynchronized array of dipoles range from 22 to -50 units in the same scale. In fact, while the averaged field patterns generated by desynchronized arrays of dipoles must be much weaker than those generated by synchronized dipoles, the instantaneous (non-averaged) patterns of both types may be equally strong and,

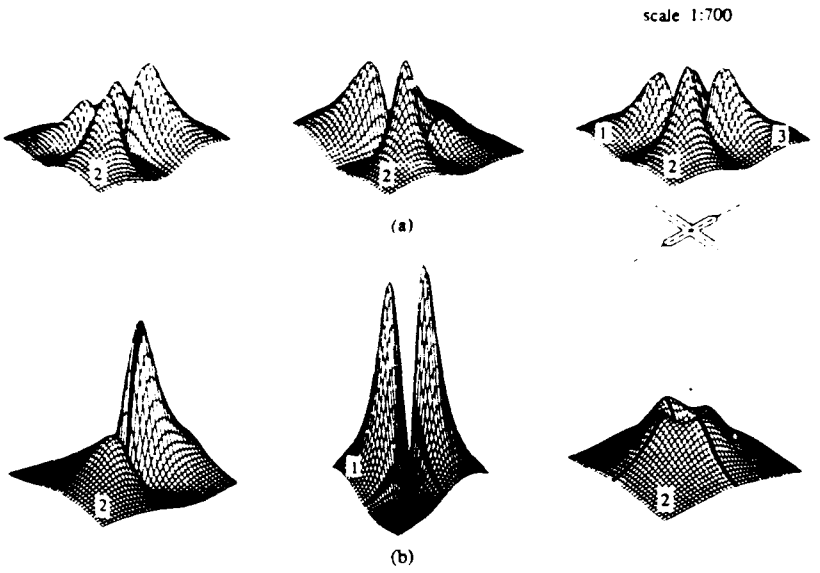

Figure 9: Field power (square of the magnetic field) patterns indicated by height above the base, corresponding to field patterns of the previous figure. Synchronous arrays of dipoles were used to produce the instantaneous patterns shown in the upper left-hand set of patterns, and, on the right, an average of 100 such patterns. Note the consistent four-lobe pattern. Numerals denote the locations of quadrants in the underlying cruciform structure, depicted at the upper right. Note the spatial extent of the power pattern is much greater than the size of the cruciform. (b) Asynchronous arrays of dipoles were used to produce the lower left-hand instantaneous patterns, with an average of 100 such patterns shown at the right.

in some instances, the patterns associated with desynchronization may even be stronger. This is made quite obvious when *field power* is averaged rather than field, albeit with the loss of information as to the direction of the field.

Field power is simply the square of the field. Figure 9 contains several samples of instantaneous field power plots similar to the isofield patterns of Fig. 8 but presented as 3-dimensional graphs. All graphs in this figure are drawn to the same arbitrary scale. In this case, 1:700 is the scale of the z-axis, where 1 unit along the a-axis is equal to 700 units of power. Thus, in each graph the z-axis is proportional to field power, and the other two axes represent distances in mm across the plane onto which the original field data were projected. It is obvious from the graphs at the bottom left that at any instant of time the locations of the regions of greatest power are quite variable, depending upon the specific array of desynchronized dipoles. The regions of greatest power tend to circulate about the center of the graph from one stantaneous plot to the next. However, a plot of average power reveals invariant features not present in single plots based upon particular distributions of dipole moments.

Figure 9 contains mean square field plots based on averaging 100 different power patterns for both the synchronized and desynchronized condiditon. In both plots the maximum power is the same order of magnitude, although there are differences in their topographies. Nev-

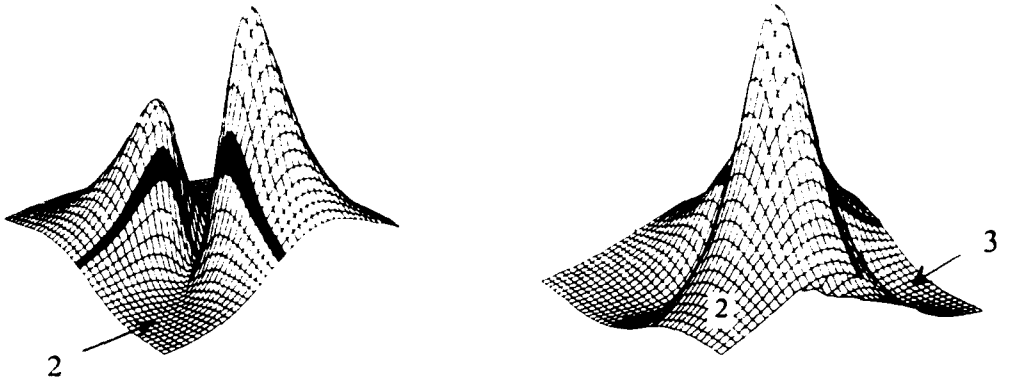

Figure 10: The same random arrays of synchronized dipoles as in the preceding figure, but with activity of dipoles of one quadrant of the cruciform structure attenuated. The plot on the left was generated with quadrant 2 of the cruciform structure attenuated by a factor of 10, and the plot on the right with quadrant 3 attenuated by the same factor. The resulting power patterns have only two extrema and not four, and have markedly greater power (the scale is 1:20,000 as opposed to 1:700 in the previous figure).

circular regions of greatest power has 4 relatively shallow peaks, although only two peaks of much greater power are present in the two instantaneous plots on the left. As shown in Fig. 11, despite the presence of a suppressed quadrant, two peaks of varying power are present in the instantaneous plots, but there is no obvious way in which these differ from the instantaneous plots of Fig. 9b. However, the right-hand mean square field plots of Fig. 11 have only three peaks when one quadrant is suppressed, and, as we have seen, there are four peaks when all quadrants are active. *Nevertheless, the visual differences between the* patterns are slight and interpretaions are possibly affected by subjective judgement. In spite of this, an objective method for identifying the suppressed region and determining its depth can be developed.

According to the superposition principle, the net field at a point in space is the linear sum of the fields of all of the contributing generators at that point. Therefore, the contribution of any portion of the cruciform structure to the total field is equal to the difference between the total field and the field generated by the portion whose level of activity is suppressed. For example, suppression of activity of one quadrant of the total structure would result in a net field pattern that differs from the pattern that arises from the activity of the total pattern prior to suppression. Hence, the pattern derived by taking the difference between the pattern measured during suppression and that prior to suppression would reveal the contribution of the suppressed portion. Of course, this is not strictly true when correspoinding differences between mean square field patterns are taken. In fact, the difference between the mean

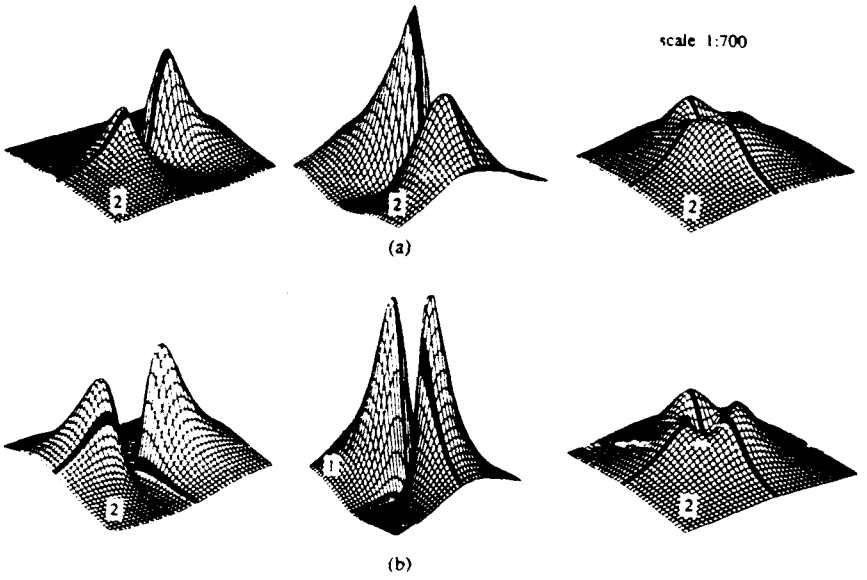

Figure 11: (a) The two instantaneous power plots on the left were obtained with asynchronous generators and with activity of quadrant 2 attenuated by a factor of 10. The right hand plot is an average of 100 such plots. (b) Similar instantaneous and averaged power plots but with activity of quadrant 3 attenuated by a factor of 10. The darkened cells are directly over the projections of the lateral fissure and calcarine sulcus of the cruciform structure. Instantaneous patterns are highly variable, and mean patterns also show variability but it is difficult to see which quadrant is suppressed.

square field patterns obtained with all quadrants active and with one quadrant suppressed contains cross terms in the vector products of the fields originating from each of the two sets of dipoles. However, if the moments of well separated sources are uncorrelated as compared with adjacent sources (as they are in this case), the contributions of the cross products to the difference between mean square fields tends to zero because of averaging. We have verified this in the present simulation by taking differences between individual field patterns with all quadrants active and with one quadrant suppressed, squaring the difference patterns and then averaging them. The resulting patterns are virtually indistinguishable from those derived simply by taking differences between the corresponding mean square field plots, which are shown here.

The reason for our emphasizing field power is that averaging the field can result in cancellation of information contained in the individual patterns included in the average. Field power, however, is additive. This makes it possible to ignore changes in the sign of the field and preserves much of the information present within single patterns when means square field is computed. This includes information related to specific regions with suppressed activity. Therefore, to determine the position and depth of a suppressed quadrant, we subtract the mean square field obtained with the suppressed quadrant from the mean square field obtained with all quadrants active, as shown in Fig. 12. These power plots were obtained with three different suppressed quadrants. The locations of these quadrants in the underlying model

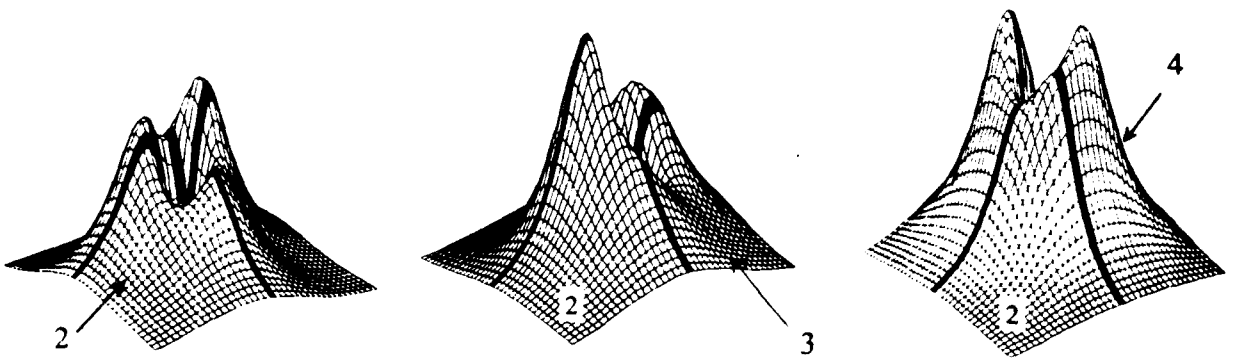

Figure 12: The result of subtracting the average power with one quadrant attenuated (as in the previous figure) from the average power with four quadrants equally active. The three "difference" patterns were obtained with quadrants 2, 3, and 4 respectively attenuated. These patterns clearly differ, depending upon which quadrant is attentuated. The angular separations between the prominent two lobes in each plot gives information on the depth of the suppressed region. The minima between the two extrema in each pattern are located over the suppressed quadrant, but are slightly offset from its center.

are indicated in the figure. It is to be noted that the difference plots are approximately U-shaped, with two prominent power peaks on the U. The minimum on these surfaces is located directly above the suppressed quadrant. This gives the lateral position of the suppressed quadrant. Assuming a uniform density of dipole moments wthin the suppressed quadrant, its depth should be 3.87 cm, since its most shallow boundary is 3 cm, and its most distal boundary is 5 cm from the surface. By measuring the angular distances between the power maxima in all three graphs we find the depth to be 3.17, 3.43 and 3.49 cm from the surface for quadrants 2, 3, and 4, respectively.

To use this same procedure in locating still smaller suppressed regions of the structure, the level of activity of a 1 cm deep portion of one quadrant, rather than the entire quadrant, was attenuated. This was either the portion of the quadrant closest to the surface of the sphere or the one closest to the center of the sphere (Fig. 4). Does suppression at different depths differentially affect the external field pattern?

Figure 13 gives the results for suppression of the shallow (Fig 4a) and deep (Fig 4b) portions of one quadrant of the overall array of asynchronous generators can deep portions of but one of the quadrants. Replication with the other quadrants gave essentially the same results. The difference plots reveal that the net power associated with the deeper structure is less than that attributable to the shallower structure, as is to be expected. Moreover, there is an easily discerned difference in the separations of the extrema in the two power difference

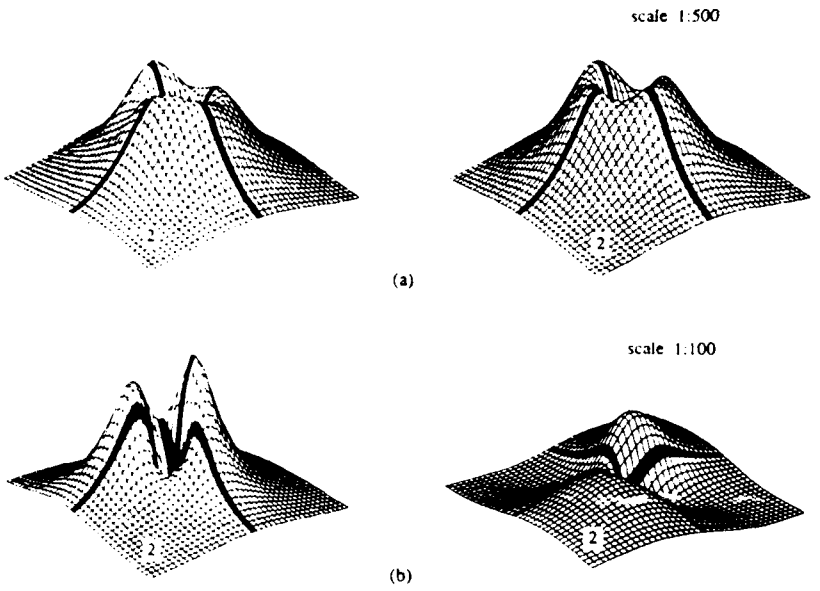

Figure 13: (a) Two average power plots obtained with, from left to right, the shallow and deep portions of one quadrant attentuated. (b) Differences between the average power plots with all quadrants active and the average power plots with the shallow portion (left) and deeper portion (right) of one quadrant suppressed. Note the wider separation between the two lobes in the latter pattern. This angular separation gives the depth of hte relatively inactive portion of the structure.

plots. The extrema associated with the deeper structure are more widely separated and of lower magnitude. It is to be noted that these differences in power and in space between extrema are related to a relatively inactive portion of cortex, and not to a relatively more active portion of cortex, as in the case of sensory evoked responses.

3.2.3 Increments in Magnitude of Asynchronous Activity

The flexibility of this type of model makes it possible to envision possible but as yet unobserved phenomena. For example, modelling an evoked response required some arbitrary assumptions. These were that the background activity is at least as strong as the evoked activity, and that it changes over time at every point in the structure. This assumption required us to adopt the asynchronous model of backgorund activity. Since the evoked response was not allowed to contribute a spatially changing pattern to the oaverall field, we opted to model it as a synchronized region. Afterwards the solution to recover the evoked response and determine the location of its generators was relatively simple and conventional. Averaging field alone recovers the source. However, this also allowed us to think about the other possible kinds of stimulus-related activity. For example, it is possible that a sensory stimulus simply results in an increase in the amount of activity within a region of cortex, without altering its statistics. In this case, both the background and the effected area could be composed of randomly oriented dipoles of random magnitudes, but the average activity

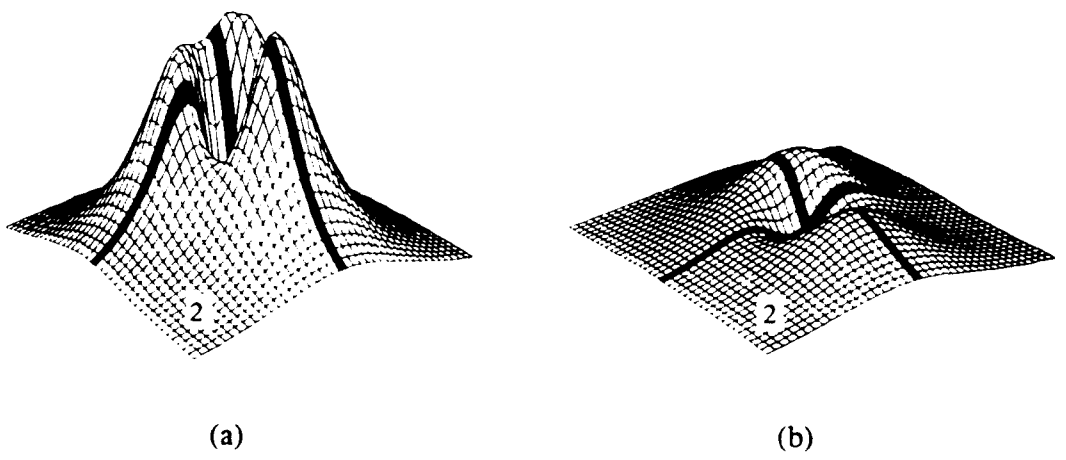

Figure 14: Average power plots with a shallow portion of quadrant 2 having asynchronous activity incremented and a deeper portion of the same quadrant of asynchronous activity also incremented.

within the affected area would be greater than it was prior to the hypothetical stimulus. Simply averaging the field patterns would not reveal such a response or its source.

As shown in Fig. 14, the incremented activity of a 1 cm deep portion (Fig. 4a) or shallow portion (Fig. 4b) of one quadrant of the overall array of asynchronous generators can be detected provided that the power is averaged. As demonstrated in Fig. 8, when the dipoles are asynchronous, the average field pattern converges toward a residual noise level, and this would be true even if the net activity of a portion of a subset of the asynchronous dipoles were less active than the other members of the set. Furthermore, after averaging power the depth of the active region can be computed simply by measuring the angular separation between the extrema and using the standard formula. Averaging field rather than power could not produce such consistent results.

3.3 Summary

The major conclusion we draw from this theoretical development is that the notions of synchronization and desynchronization can be transcribed into a theoretical framework with respect to which the spatial aspects of the phenomena may be interpreted. Simple magnetic field or electric potential measurements may not be informative, especially since averaging may not reveal the evolution of field patterns over time. However, power measurements do permit time averaging of samples of MEG or EEG, and these may reveal invariant spatio-temporal properties described above. These invarient properties may well be related to mental states of subjects as well as the types of stimuli employed. Thus, when subjects engage in some mental tasks and suppression or enhancement of the sponteneous activity of different regions of the brain does occur, then taking differences in field power patterns can make it possible to locate and identify the affected regions.

In principle, the brain may be affected in different ways by sensory stimuli or by mental

operations associated with them. Yet not all of the states of the brain may be revealed by straightforward signal averaging. For example, the mere increase or decrease in the level of synchronous activity of a region of the brain could be revealed by averaging MEG activity time-locked to the stimulus. However, if the affected region is asynchronously active it will not contribute to the average response, although it could contribute to mean square field patterns and the differences among them. This is consistent with observations that average levels of the "noise" of some regions of the brain do change in step with evoked responses of the EEG [43] [42] [82]. If it can be verified in practical situations that both decrements and increments in this background activity may now be traced to specific brain regions, then it would raise the tantalizing possiblity of performing genuine functional brain imaging using the MEG to complement similar efforts involving PET.

4 Spatial Extent of Sensory Evoked Cortical Activity

4.1 Introduction

Rapid progress has been made in the past decade to exploit the capabilities of magnetic source imaging the purpose of providing quantitative information on sensory-related activity of the human cortex. One of the benefits is a measure of the *strength* of neuronal activity, as provided by the moment of the current dipole best accounting for a field pattern. Comparison with mathematical representations of stimulus-related functional sequences, such as the tonotopic [93] [95] [33] and amplitopic [79] loci across primary auditory cortex, suggest that the strength of neuronal activity is independent of physical attributes of the stimulus, provideed that the stimulus is robust. Since magnetic measurements indicate that the net neuronal intracellular current lies perpendicular to the local cortical surface, it is generally accepted that the responding currents arise from pyramidal cells.

However, at noise levels encountered in typical magnetic measurements, it is not possible to differentiate between magnetic field patterns generated by cortical sources of different spatial extent of activity unless the spread of activity is at least comparable to the distance to the nearest sensor - typically several centimeters (Okada [77]). The extent of cortical involvement is an important issue when considering possible models for neural networks that would account for observed signals. Consider that the just-noticeable difference for pitch in human auditory studies corresponds to a shift of the center of activity by $\sim 10\,\mu m$ along the tonotopic axis, and the just-noticeable difference for loudness to a shift of $\sim 100\,\mu m$ along the (approximately orthogonal) amplitopic axis [119]. Then if cortical response strengths were determined experimentally to correspond to an active cortical area on the order of $1\,cm^2$, it would be unrealistic to interpret the psychophysical measures as reflecting a columnar organization, with activity limited to the column of best frequency and amplitude. Instead, neuronal populations responding to distinguishable frequencies or intensities must be largely overlapping across cortex.

4.2 Analysis of Current Source-Density Data

As a first step toward determining the spatial extent of evoked cortical activity, we utilized data on current source-density analyses in the somatosensory cortex of macaque monkey

to determine the corresponding current-dipole moment that characterizes the activity underlying 1 mm^2 of cortical surface during moments of peak activity. A similar analysis was carried out with published data on visual cortex of the cat. The close correspondence in results prompted us to report these values as a first step toward establishing a quantitative relationship in higher mammals between physiological activity of sensory cortex and macroscopic measures provided by the electroencephalogram (EEG) and magnetoencephalogram (MEG). We also suggest that this measure of cortical activity may well characterize human sensory functions as well, for reasons to be given at the end of this section.

We have analyzed electric potential data obtained by other researchers who employed arrays of microelectrodes extending through the depth of sensory cortex of two animal species – the cat and macaque monkey. For latencies of peak response we compute the net current-dipole moment per square millimeter of cortical surface area. Comparing this with observed values for the total current-dipole moment obtained from neuromagnetic studies of human subjects, we estimate the corresponding area of human cortex that overlies the observed coherent neuronal responses. An earlier study by Okada [78] of the neuromagnetic field evoked by electrical stimulation of cells in a slice of turtle cerebellum *in vitro* provides an example where excellent quantitative agreement with only 20% discrepancy is obtained between intracortical potential measurements and the external magnetic field strength on the basis of present theory.

As material we have chosen recent electrophysiological studies of sensory evoked activity of cerebral cortex that characterize with comparatively fine resolution the current source density (CSD) at various depths. The data are those of Mitzdorf (1987) [69] for visual cortex of cat, Mitzdorf and Singer (1979) [70] for visual cortex of macaque monkey, and Cauller and Kulics (1990) [8] for somatosensory cortex of macaque monkey. We shall describe our method by reference to the data of Mitzdorf (1987) obtained in penetrations through visual areas 17 and 18 in cat, which are representative of many close inspections of several thousand CSD profiles. Several stimuli were employed. One was a double reversal of a grating with spatial frequency of 0.5 cycle/deg, presentation time of 100 ms, and interstimulus interval of 1200 ms. Figure 15a illustrates the depth dependence of the observed field potentials at long latencies recorded at 150 μm intervals within area 17. The corresponding depth profile of the current source-density is shown in Fig. 15b. These traces represent the density of current appearing in the extracellular space from the intracellular medium at the indicated depth, as given by the negative of the second derivative of the variation of extracellular potential with depth (Mitzdorf 1987).

For simple geometries, the predominant source of extracranial magnetic field is the *intracellular* current, as evidenced by the relative polarities of sensory evoked potentials and magnetic fields (Hari *et al.* [28]) and studies of isolated nerve preparations (Wikswo *et al.* [117], Swinney and Wikswo [110], Plonsey [89], and Roth and Wikswo [96]. The intracellular current flows in the opposite direction to that of the extracellular current. Since the distribution of current source-density was nearly invarient parallel to the laminae, we computed the intracellular current per unit area of cortical surface flowing perpendicular to the laminae at each depth (illustrated in Fig. 15c) by reversing the sign of the current source density, integrating it from the most superficial electrode to the deepest electrode, and multiplying by the conductivity of the medium for translaminar current flow (We used the value 0.5 $\Omega^{-1}\, m^{-1}$ for the conductivity, which is established with an uncertainty of about

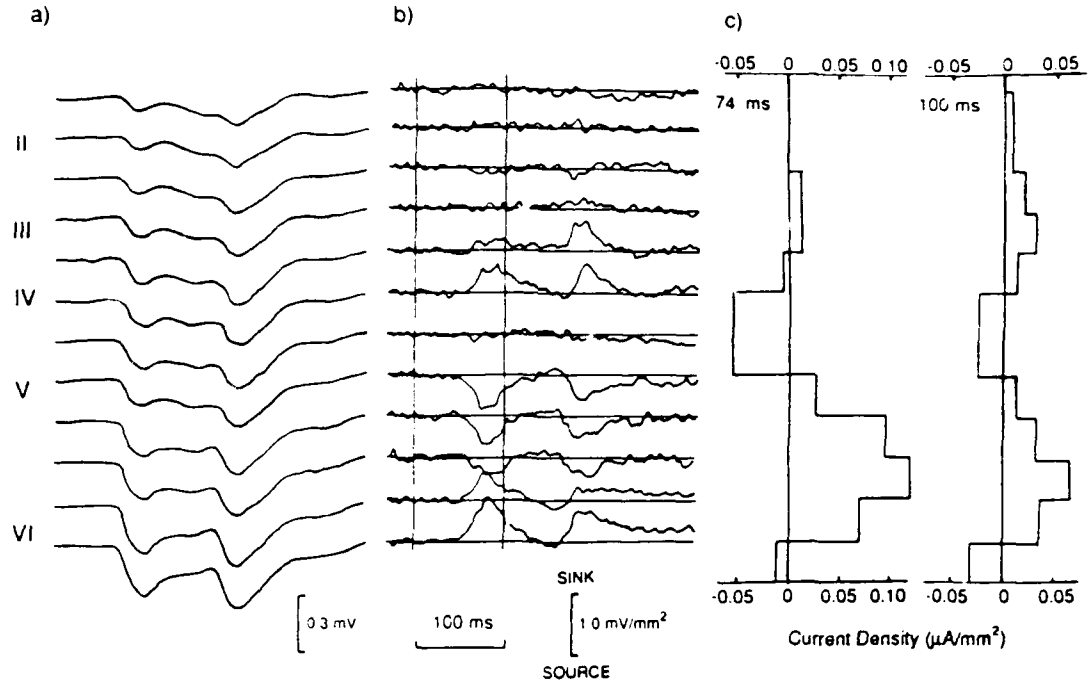

Figure 15: (a) Field potential measurements shown for 150 μm depth intervals in visual area 17 of cat in a cortical area responding to a double reversal of a grating, with receptive field within the central 3 deg, and (b) computed current source density profiles in the *extracellular* medium where sinks are indicated by upward deflection, with times of pattern reversal denoted by the two vertical lines (adapted from Mitzdorf 1987). (c) Computed profile for the trans-laminar *intracellular* current density, averaged over 150 μm depth intervals for responses at 74 and 100 ms. Integration of current source-density was from surface of cortex to depth, with positive sign indicating current directed toward the surface.

$\pm$ 15%.). The net current-dipole moment-density, expressed as the current-dipole moment per square millimeter of cortical surface area, was obtained by integrating this intracellular current density over the same path. As a measure of control, we computed the total current entering the intracellular space and compared it with the total current that leaves, both per unit area of cortical surface. With ideal data and accurate analysis, the two should be equal. The ratio of their difference to the average of the two values is called the "current imbalance", and this value when expressed as a percentage serves as a measure of error in the procedure. Figure 16 lists representative values in the third column. The effect of current imbalance on the deduced current-dipole moment-density is obtained by comparing the results of computing the values of the latter in two ways: integrating into the depth of cortex and by integrating from the bottom to the superficial layer. These respective values are shown in the fourth column.

The most likely reason for obtaining large non-zero values of current imbalance for two

Stimulus	Latency (ms)	Current imbalance (%)	Dipole moment per unit area ($pA \cdot m/mm^2$)	
			Downward	Upward
Movement of grating (Area 17)	76	15	96	67
	152	32	-104	-48
	228	42	118	24
Movement of grating (Area 17)	141	21	72	37
	193	24	57	38
	259	14	76	49
Double reversal of grating (Area 17)	74	9	35	17
	100	28	-44	-12
	183	50	51	-51
Appearance of grating (Area 18)	80	16	34	74
	100	-30	113	47
	160	17	75	26
	200	0	25	25
Appearance of grating (Area 18)	100	-10	81	54
	500	25	140	62
	560	2	25	31

Figure 16: Visually evoked responses in the visual cortex of cat. In the right-hand column, the first value for the current-dipole moment-density is obtained by integrating the deduced intracellular current from the most superficial electrode to the deepest and the second value by integrating in the opposite direction. Positive values indicate moment directed toward cortical surface. Analysis of data of Mitzdorf (1987).

of these components, as well as for several other components given in Fig. 16, is that the array of electrode positions did not properly sample all neuronal sources or sinks, particularly in superficial layers. In addition, typical length constants describing the variation of intracellular current along dendritic branches into the depth of cortex are about $100\,\mu$m, which implies that electrode spacings greater than this will miss details in the transcortical potential profile. This problem is accentuated when the current source-density is computed by taking the second spatial derivative of the profile. Other complications may arise from the influence of efferent and afferent fibres on the local conductivity, but there is no gauge as yet for the magnitude of this effect.

Numerical values for the computed current-dipole moment-density are summarized in the right-hand column of Fig. 16 for a variety of responses of cat to visual grating stimuli. The units for current-dipole moment-density are expressed as picoampere-meter per square millimeter of cortical surface ($pA \cdot m/mm^2$). The effects of boundaries separating media of differing electrical conductivity may also contribute to the magnetic field outside the scalp. One such "secondary source" is where the pattern of extracellular current of a neuron is perturbed near the outer surface of its membrane. This has the effect of enhancing the

field produced by the intracellular current and has been considered by Okada (1989) [78] in studies of a slice of turtle cerebellum *in vitro*. As this effect appears to provide only a $\sim 10\%$ contribution to the observed field, it was neglected. Another secondary source is the pial membrane covering the cortical surface. Because the electrical conductivity of cortex is less than that of cerebrospinal fluid outside the membrane, there is a net secondary current source distribution along the membrane pointing in the same direction as the cortical dipole moment. This effect may indeed be very large and produce a field that is comparable to that of intracellular currents, as evidenced by their studies of cerebellar tissue in a bath of physiological saline. However, for cortical sources in sulci and fissures this contribution will be cancelled by an oppositely directed secondary source in the facing sulcal wall [34] and therefore need not be considered further.

Our analysis did not distinguish between different cell populations in cortex that contribute to the dipole moment, for instance pyramidal cells of overlapping dendritic trees whose cell bodies lie in different cortical layers. We considered only the total intracellular current at each depth of cortex. However, we should note that comparisons of extracranial magnetic fields with current source-density profiles during direct electrical stimulation of cortex of rat provide a means of identifying separate contributions (Barth and Sutherling [3]).

It is noteworthy that markedly greater current-dipole moment-densities may be obtained for direct electrical stimulation. We have analyzed data of Mitzdorf and Singer (1979) on the macaque monkey where electrical stimulation was applied to the optic chiasm. Figure 17 shows that the corresponding current-dipole moment-density for a short-latency response is typically about 10 times greater than those for natural stimuli characterized in Fig. 16. How much of this difference may be attributed to differences between short-latency and long-latency characteristics remains to be determined.

We have also analyzed current source-density studies for the monkey obtained in somatosensory studies by Cauller and Kulics (1990). Measurements were reported for $200\,\mu$m intervals into the depth of cortex at the crown of the postcentral gyrus of two awake monkeys, with special care to ensure that the penetrations were perpendicular to the pial surface (to within 13^0). This location corresponds to the projection of hand representations in somatosensory areas 1 and 2. Responses to separate mechanical and electrical stimulation of the receptive field center of the palm or finger were recorded. Figure 18a,b illustrates responses to mechanical stimulation of finger IV. Using these data we computed the percentage current imbalance as described previously for cat, by comparing the difference between the total source and total sink of intracellular current with the average of their absolute values. These imbalances are shown as a percentage in Fig. 19. Similarly we computed the translaminar intracellular current per unit area of cortical surface, as illustrated in Fig. 18c. Integrating through cortex downward and then upward provides two measures for the current-dipole moment-density as summarized in the right-hand column of Fig. 19.

4.3 A Perspective

The purpose of this analysis is to determine whether there is sufficient uniformity in the strength of sensory evoked, spatially coherent cortical activity in mammals to establish an estimate for a "typical" level of activity. Although the conclusions we shall draw are based on

Stimulus	Latency (ms)	Dipole moment per unit area ($pA \cdot m/mm^2$)
Electrical stimulation	10	400
	12	-140
	14	390

Figure 17: Early components of the electrically evoked responses in the visual cortex of monkey. Positive values indicate the dipole moment is directed toward the cortical surface. Analysis of the data of Mitzdorf and Singer (1979).

this limited set of data, the agreement we obtain across the two species and sensory modalities for long latency responses is sufficiently strong to suggest a more general applicability. A useful measure for activity is the current-dipole moment-density representing the integral of intracellular current through the thickness of cortex, per unit surface area. Variability in this measure may be expected, because the number of participating neurons could depend on the task required and also because response strength in sensory cortex, as measured by the total current dipole moment, is influenced by many factors such as attention (Curtis *et al.* [16]) and adaptation (Yamamoto *et al.* [124]).

Nevertheless, it is remarkable that despite these considerations, the limitations in the accuracy of our analysis, and the fact that data from different species and sensory modalities were included, all of the estimates in Tables 1 and 2 lie within a factor of ~ 2 of the value $50\,\mathrm{pA \cdot m/mm^2}$. We obtain a more reliable gauge if we restrict attention to those values that are established with highest confidence, *viz.* to those where the current imbalance is less than 25%. Confining attention to these in Table 1, we take for each condition and latency the average of values computed by integrating upward and downward through cortex. Then the average of the magnitudes across conditions and latencies is $53\,\mathrm{pA \cdot m/mm^2}$ (S.D. = 28). This is remarkably close to the average obtained in the same way for the values in Table 3: $66\,\mathrm{pA \cdot m/mm^2}$ (S.D. = 33). We conclude that a representative value for natural stimuli at suprathreshold levels could be taken as $50\,\mathrm{pA \cdot m/mm^2}$ with an uncertainty of a factor of 2 above and below that value. Enhancement in strength by an order of magnitude is shown in Table 2 for short-latency responses to a stimulus that is not normally experienced, *viz.* electrical stimulation of white matter in the visual system of monkey.

We now argue that these values for long-latency responses may well be representative of sensory-evoked activity in human cerebral cortex, aside perhaps from the primary visual area.

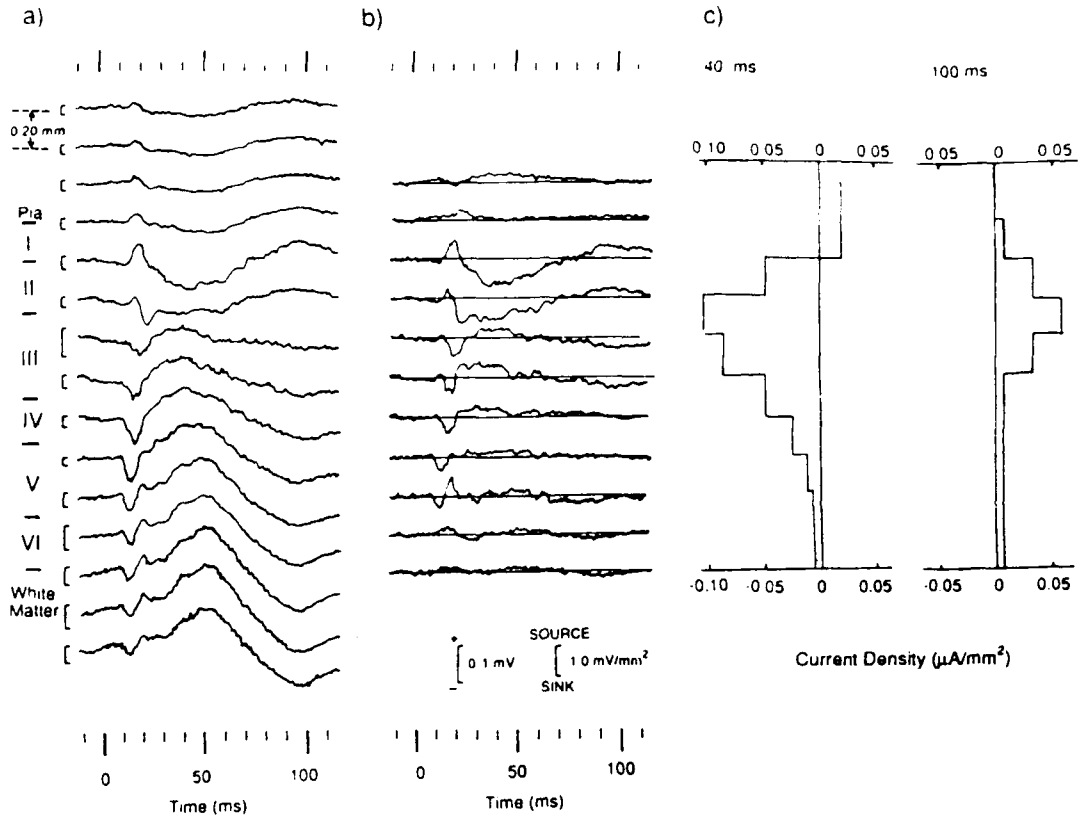

Figure 18: (a) Field potential measurements at 200 μm depth intervals in somatosensory area SI of monkey, in response to mechanical stimulation of the receptive field center of finger IV, and (b) computed current source density profiles in the extracellular medium with sinks indicated by downward deflection (adapted from Cauller and Kulics 1990). (c) Computed profile for trans-laminar intracellular current density, for 40 and 100 ms latencies. Integration of current source-density was from surface of cortex to the depth, with positive sign indicating current directed toward the surface.

Our justification is the similarity of cell density for cat, macaque monkey, and human. Rockel *et al.* [91] concluded that except for visual area 17 of primates there is a basic uniformity in cortical cell density across species. This conclusion was based on observations for a variety of species that about 110 neurons are found in a 30-μm-wide by 25-μm-length strip of cortex, from either motor, somatosensory, primary visual, frontal, parietal or temporal areas. About 75% of these cells are pyramidal cells. The only exception to the common neuron count of Rockel *et al.* occurred in the binocular region of area 17 in primates, where about 2.5 times more neurons were found than in other areas. The comparable level of evoked current-dipole moment-density that we deduce for macaque somatosensory cortex and cat visual areas 17 and 18 suggests further that the neuronal activity levels across these species are similar. We propose therefore that a typical value of 50 pA·m/mm^2 is appropriate for the current-dipole moment-density of long latency components in human cortex as well. This comparative uniformity of cortical response across species may well be limited to suprathreshold stimuli, where cortical response levels are insensitive to stimulus strength. When a stimulus is

Stimulus	Latency (ms)	Current imbalance (%)	Dipole moment per unit area ($pA \cdot m/mm^2$)	
			Downward	Upward
Electrocutaneous stimulation of thenar eminence	40	33	−36	−100
	50	12	−63	−108
	100	17	30	91
Mechanical stimulation of receptive field center: finger IV	40	17	−76	−121
	50	28	−74	−120
	100	10	36	22
Electrocutaneous stimulation of receptive field center: tip of thumb	40	−8	−90	−74
	80	−40	20	45
	100	40	−28	−54

Figure 19: Somatosensory evoked responses in SI cortex of awake monkey. The first value for the dipole moment per unit area is obtained by integrating the deduced intracellular current from the most superficial electrode to the deepest and the second value by integrating in the opposite direction. Positive values indicate moment directed toward cortical surface. Analysis of data of Cauller and Kulics (1990).

weakened, a level is reached where cortical response begins to decline, and the corresponding current-dipole moment-density may well be species and stimulus dependent. It is important to define these limits by future studies in other species, in primate visual areas where the cell density is higher, and in other sensory modalities. The prospect of establishing quantitative relationships between activity in animal preparations and non-invasive studies of humans should encourage continued development of current source-density techniques. In particular, attention must be devoted to solving the technical problems that appear in the present analysis as a large current imbalance between total intracellular sources and sinks for several temporal components.

Neuromagnetic studies of sensory evoked responses in human cortex reveal typical neuronal activity levels that correspond to a current-dipole moment in the range of 2-20 nA·m for middle and long-latency responses (for a recent conference proceedings, see Williamson *et al.* 1989). For the current-dipole moment-density just cited, these values correspond to cortical activation extending over a surface area in the range 40-400 mm^2. A reasonable estimate for the smallest detectible area is $\sim 10\,mm^2$, based on the weakest current dipole at a shallow depth that can be detected with the sensitivity of contemporary field sensors or electrodes. Since auditory, somatosensory, and visual cortical areas in human each comprise many square centimeters, MEG and EEG techniques are capable of monitoring comparatively confined cortical excitations.

However, even $10\,mm^2$ is a much larger area than certain length scales of organization in human cortex. One example is the $10\,\mu m \times 100\,\mu m$ module that would be required to

provide a columnar mosaic across the tonotopic and amplitopic surface of human auditory cortex, if the centers of contiguous columns are spaced by dimensions that are characteristic of just-noticeable differences in pitch and loudness. An important implication of this finding is that neuronal activity in human auditory cortex evoked by the onset of a tone burst is largely overlapping for these close-lying but distinguishable attributes of the stimulus.

It is of some interest to consider the prospect that activity could be observed in such a small region as a macrocolumn of visual cortex, with the dimension of about $800\,\mu m \times 800\,\mu m$ (Mountcastle [71]). Unfortunately, such an area could produce a current dipole moment that is an order of magnitude too weak to be detected by present magnetic techniques. While the continuing development of magnetic sensors for human studies may ultimately provide this sensitivity, the first success is more likely to come in animal studies where the detection coil can be placed much closer to the neuronal source (Wikswo *et al.* [116]). A miniaturized sensing system with the detector only 1.5 mm from the exposed cortical surface is expected to provide this advantage [6].

5 Cortical Responses to Chrominance and Luminance Stimuli

In the first year of this program Krauskopf, Klemic, Lounassmaa, Travis, Kaufman, and Williamson [47] reported on the results of a study to determine whether pure chrominance changes affect cortical areas that are not affected by luminance changes. (Travis was a post-doctoral student supported by the URI program at NYU, and Klemic a graduate student.) In color vision the first stages, at the level of the receptor mechanisms, are now fairly well understood, and research by Krauskopf and his colleagues in the psychophysical domain [48] and the physiological domain [19] has helped to clarify the nature of the second stage opponent mechanisms. It is clear that the parvocellular lateral geniculate layers consists of two major types of center-surround chromatically opponent units. Lennie et al. [54] applied the same electrophysiological methods to cortical units as were used to study lateral geniculate units, and found cells tuned to respond best to isoluminant stimuli in many different directions around the color circle. Detailed analysis of psychophysical habituation experiments and results of experiments on the discrimination of threshold changes in color also point to the existence of higher order mechanisms tuned to many different directions in color space.

5.1 Pathways for Color Processing

Previous clinical [5, 97], physiological [53][125] studies suggest that at certain stages chrominance and luminance information is processed by separate neuronal populations. The cortical areas where segregated activity takes place have not been fully defined. Shapley [106] has recently provided a review of the pathways from retina to cortex. Single-cell recordings on monkeys [19] indicate that at the earliest stages of processing magnocellular and parvocellular cells in the lateral geniculate nucleus (LGN) receive different chrominance information from retina. The two populations of these cells are physically distinct but are separated by only a few millimeters within the LGN. Magnocellular and parvocellular projections to striate cortex V1 appear to be somewhat segregated. Cortical neurons with high contrast gain (a property exhibited by magnocellular cells) are found in layer IV$c\alpha$, whereas neurons

exhibiting color-opponent responses (a feature emphasized by parvocellular cells) are in layer IV$c\beta$.[30] There is some evidence that magnocellular and parvocellular signals converge on a network of cortical patches ("blobs") in layers II and III. [111] Many cells within the blobs are color selective [56, 57] but so are some within interblob regions [54]. Neurons within the blobs project to sets of neurons whose locations form stripes across cortical area V2, and neurons of the inter-blob region project to a second set of stripes [108]. Livingstone and Hubel [57, 55] have proposed that the blob cells and their projection to stripes in V2 comprise a system for color vision, however Lennie *et al.* [53] provide contradictory evidence. Recent positron-emission-tomography (PET) measurements [62] indicate that there are color responding areas in humans in the lingual and fusiform gyri of the occipital lobe.

Evoked potential measurements reveal temporal components whose amplitudes and latencies are affected by chromatic stimuli, and these responses vary with whether the stimulus is confined in the visual field to provide only foveal stimulation or broad-field stimulation. These considerations are reviewed by Regan [90]. Many of the earlier studies are difficult to interpret, because the stimulus field was so extensive as to excite an inhomogeneous area of retinal photoreceptors. However, since the early work of Clynes and Kohn [10] evidence has accumulated to show that the amplitudes of various temporal components of the EEG vary with the spectral distribution of the illuminant, whether the stimulus is a change in intensity or pattern. However, none of these studies has been carried out with a sufficiently fine array of electrodes to adequately address the question as to whether the location of activity in visual areas depends on whether a chrominance or luminance stimulus is employed. It is worth noting that the results of one study with color stimuli by Paulus et al.[81] used 5 electrodes to monitor EEG responses across the occipital lobe, and the results led the authors to suggest that an 87 ms component of the VEP reflects afferent activity projected from P cells of the LGN rather than intrinsic cortical activity.

5.2 Neuromagnetic Studies

Dr. Krauskopf began a collaboration with personnel in our laboratory and introduced the use of isoluminant chromatic stimuli to determine if it is possible to detect spatially separated regions in visual cortex that are tuned to respond to the different directions in color space. Thus far, microelectrode studies have not clarified this issue. In this work isoluminant red and green stimuli were presented alternately. Also, increments and decrements in luminance of white patches on a neutral background are similarly alternated. The chromatic stimuli, which are matched by means of heterochromatic photometry to their neutral backgrounds, evoked rather robust neuromagnetic fields. It was this success that lead to the study we briefly describe in this section.

In the present neuromagnetic study, two series of detailed measurements were carried out specifically to determine whether it is possible to detect differences in the locations of cortical activity for responses to chrominance and luminance stimuli. The initial set [47] was performed at New York University (NYU) with a 5-channel system of axial second-order gradiometers as detection coils. Gladys Klemic carried this out as her Masters Thesis in the Department of Physics. Also collaborating were Dr. D. Travis and Professors J. Krauskopf, L. Kaufman, and S.J. Williamson. The second set of studies was carried out at the Helsinki University of Technology (HUT) with a 24-channel system of planar first-order gradiometers.

In addition to Gladys Klemic, the collaborators at HUT were Drs. S. T. Lu, S. Ahlfors, R.J. Ilmoniemi, and Professor O.V. Lounasmaa, Director of the Laboratory.

In the first study at NYU, two classes of stimuli were generated with a personal computer with a VGA board and projected by means of an Electrohome video projector onto a screen inside a magnetically shielded room. With the subject fixating eyes on a black dot in the middle of the screen, both chrominance and luminance stimuli were presented against a neutral surround as a disc of 0.5 deg diameter displaced by 1 deg in the lower-left visual field. The red and the green stimuli were made equiluminant with the background by means of heterochromatic flicker photometry for each subject. The luminance stimuli were presented as a black or white disc against the same neutral surround. Red, green, black, and white stimuli were shown in random order, each for a duration of 360 ms with an interstimulus interval of 600 ms.

The magnetic field was measured at 60–65 positions over the occipital and parietal areas of the head, for each of three subjects. Responses were sampled at a rate of 128 Hz and bandpass filtered for the range 0.5-100 Hz for subsequent processing by a Hewlett Packard 9000 Model 350 computer. Measurement locations were determined by the Probe Position Indicator system [124], which interprets signals induced in sets of small coils attached to a head band on the subject when ac currents are fed to a set of coils mounted near the sensors. Averages of 100 responses for each stimulus condition at each position were subsequently computed and filtered for the range 1-20 Hz.

Stimuli in the study at HUT were based on the same principles, but generated by a Macintosh II personal computer and included some important new features. The stimuli were presented in random order with a duration of 600 ms, followed by a random interstimulus interval (ISI) between 400–1000 ms. The subject fixated at a small cross in the center of the screen. Since some visual areas are organized retinotopically and since radially oriented or deep sources are not detected magnetically, it is conceivable that some stimulus presentations would elicit larger measurable fields than others and thus be more suited to the neuromagnetic technique. For this reason, the stimulus size (from 0.5 to 5.0 deg of visual angle) and location in the visual field (lower quadrants and center) were varied.

Four other configurations were also explored to find the optimal chrominance stimuli: red circle on an equiluminant green background, red-and-green equiluminant gratings, a so called "Mondrian" pattern [49, 62], in which one region at a time changed chrominance or luminance, and finally a "subtraction" paradigm. In the subtraction study, a green spot was shown against a less luminant gray background. The green spot, however, was equiluminant with a white spot that was subsequently presented against the same gray background. In this way, both stimuli had the same luminance component while the green spot had a chrominance signal as well. The difference in response to these two stimuli was calculated, the idea being that the response to all components besides chrominance would cancel out, leaving the chrominance signal.

Seven subjects were measured in a magnetically shielded room. All were first tested, and found normal, for color vision deficiencies with a Farnsworth Dichotomous Test for Color Blindness (Luneau Ophtalmologie, Chartres, France). The stimuli were viewed, via two mirrors, through a hole in the wall of the shielded room.

The magnetic field was measured with a 24-channel magnetometer [40] over both hemispheres. The device has an array of 12 pairs of planar gradiometers, each measuring two

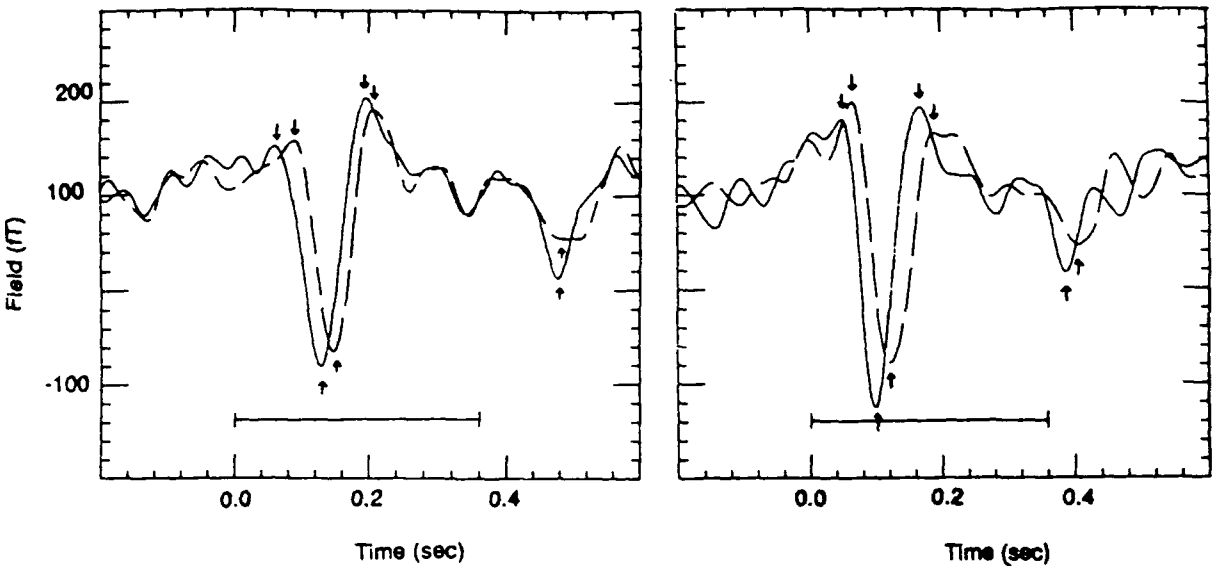

Figure 20: Average of 90 responses to *bw* (solid line) and to *rg* (dashed line) stimuli for two subjects. The stimulus duration is shown at the bottom, and components are marked with arrows. The bandwidth is 2-20 Hz.

orthogonal tangential derivatives of the radial field component. This arrangement covers an area with a diameter of 125 mm. The position of the magnetometer was determined from magnetic signals produced by 3 coils attached on the head [46], allowing us to combine measurements from different 24-channel recordings when advantageous.

After analog low-pass filtering at 100 Hz, the responses were sampled at a rate of 500 Hz by an HP1000 computer. Averages of about 100 repetitions were taken for each stimulus type, and data were subsequently computationally filtered from 0–30 Hz and analyzed to find the best equivalent dipole.

5.2.1 NYU Results

Robust magnetic responses to the appearance of chrominance and luminance responses were observed. To further improve the signal-to-noise ratio, responses to red or green (*rg*) were averaged together, as were the black and white (*bw*) responses. Three temporal components in the magnetic signal were detected for both classes of stimuli, as well as an offset response following stimulus termination. Representative responses are shown in Fig. 20.

The latencies of the response components were consistently longer for *rg* than for *bw*, typically by 10–20 ms, although response amplitudes were similar. For the first subject (S1), the peak *rg* responses appeared at about 90, 150, and 220 ms, and the peak *bw* responses appeared at 65, 140, and 200 ms. For convenience we denote the three components as P1, N1, and P2. For the second subject (S2) these latencies were 70, 130, and 180 ms and 50, 100, and 160 ms. The third subject (S3) showed similar though weaker responses. The differencies in latency were found to be affected by the relative modulation amplitudes along the *rg* and

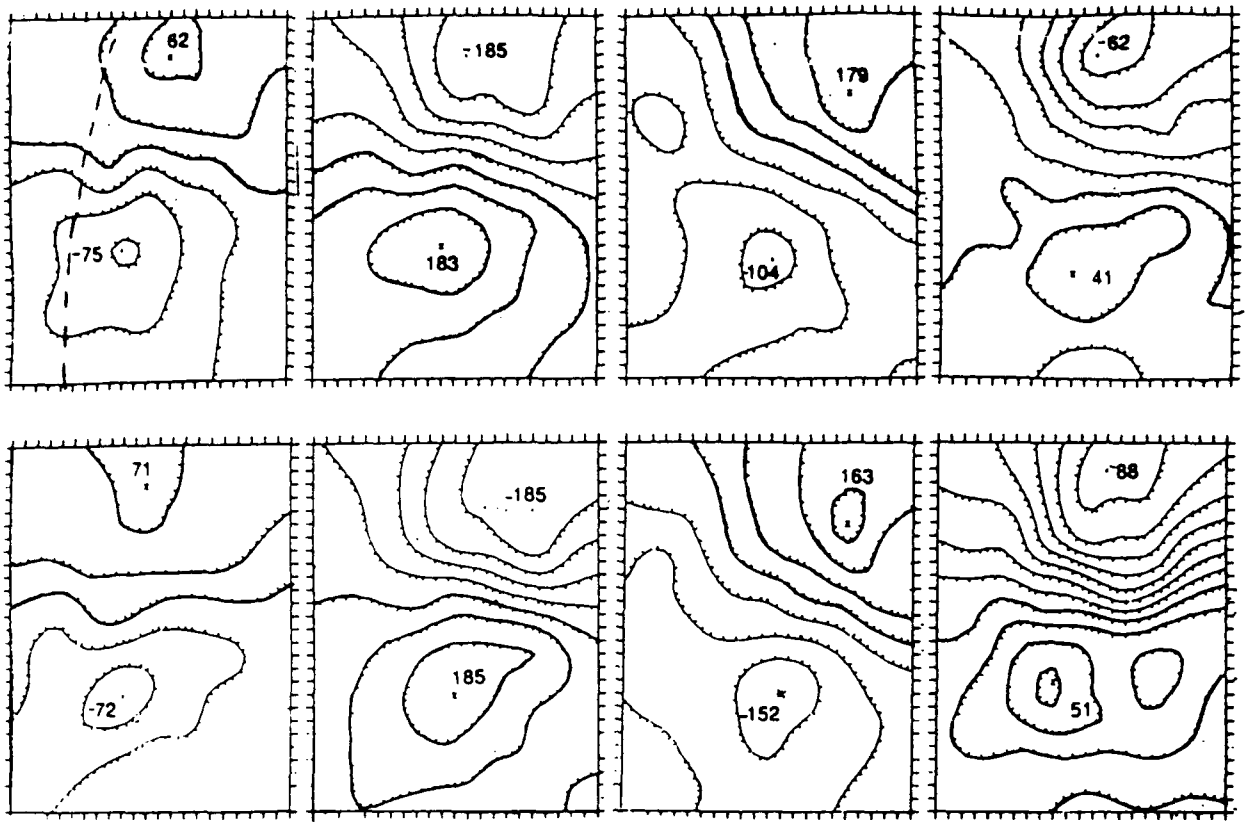

Figure 21: Isofield contour maps obtained at NYU describing the magnetic field pattern across the occipital scalp for components P1, N1, P2 and offset N1, for subject S1. Upper set of panels is for chrominance stimuli and lower for luminance stimuli. The midline is denoted by the heavy broken line in the upper left panel.

bw axes. The latencies could be made comparable when the luminance change in the *bw* condition was reduced to near threshold, thus increasing latencies for *bw* stimuli. However, at suprathreshold levels we find that chrominance information processing stages exhibited a consistent delay of about 15 ms with respect to luminance information processing.

The isofield contour maps for the three components are illustrated in Figs. 21 and 22. Most components exhibit a dipolar pattern, with one strong region where field emerges from the scalp and another where it enters. The field strength at these positive and negative extrema are of comparable magnitudes, suggesting that there is only one underlying neuronal source and it is spatially confined. For subject S1, the contour plots in Fig. 21 show no apparent difference between chrominance and luminance conditions for the three components P1, N1, and P2 following stimulus onset. The same is true as well as for the stimulus offset response. Also, in Fig. 22, there is no appreciable difference in the onset components P1 and N1 and the offset components of subject S2. However, the third onset component P2 does show an apparent difference between field patterns. Compared with the field pattern for luminance stimulation, the response to chrominance stimulation has its negative field extremum shifted to the left, and positive field extremum shifted to the right. However, the midpoint between the chrominance extrema is only slightly displaced from the position of

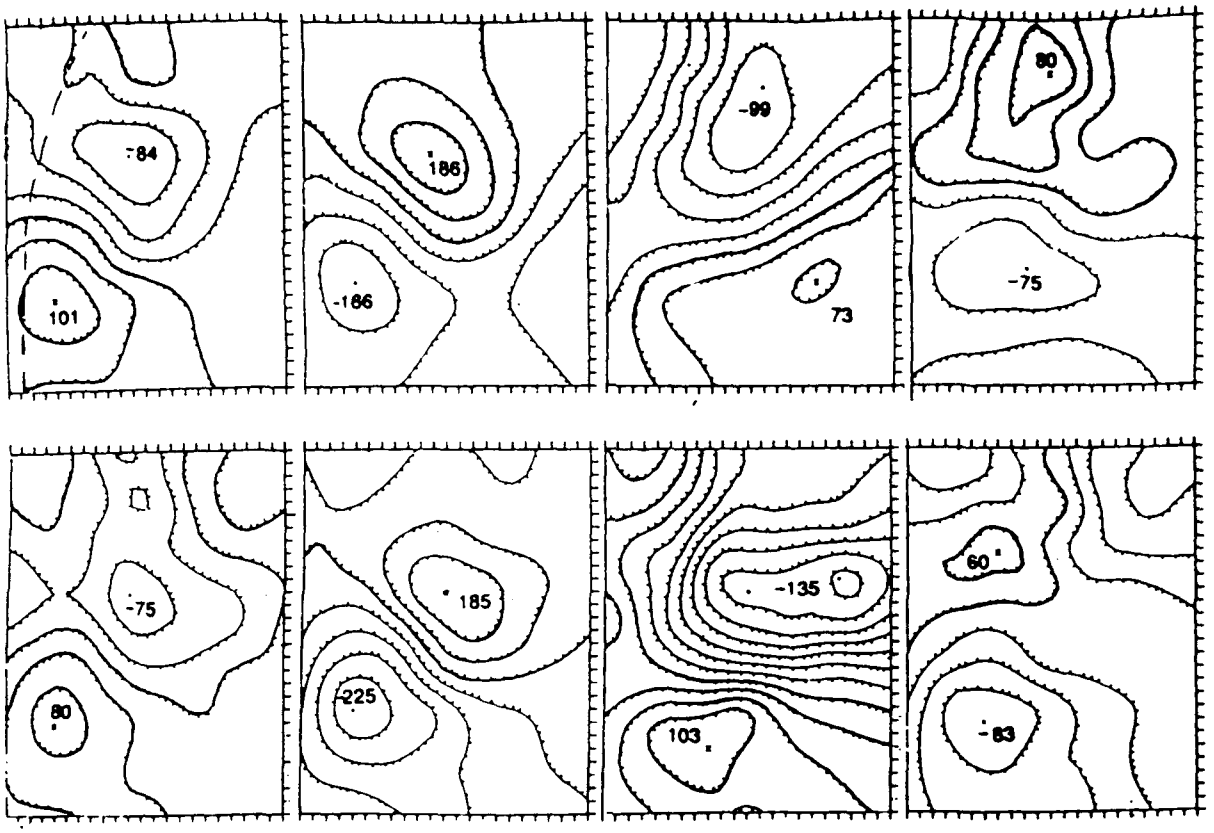

Figure 22: Similar to previous figure, except for subject S2.

the luminance extrema. This difference in patterns may be viewed as a counter-clockwise rotation of the underlying neuronal current. Such a rotation could be produced by cortical activity lying at a gyrus or sulcus, where the normal to the cortical surface rotates markedly with slight shifts in position across cortex. Therefore, a slight difference in the location of response to chrominance and luminance stimuli could appear primarily as a rotation of the neuronal current.

Such an effect, if real, would indicate that the centers of neuronal activity engaged in processing chrominance and luminance information are spatially displaced, although the active populations may well overlap appreciably across cortex. The fact that no such displacement is perceived for the responses of subject S1 could be due to a difference in cortical topography, viz. that the two centers of activity lie on a relative flat surface of cortex where a subtle difference in the location of activity would not cause the neuronal currents to differ appreciably in orientation. However, the F-ratio computed for the *rg* and *bw* data sets that served as the basis for the P2 contour plots in Fig. 22 showed no significant difference. A significant difference would be indicated for the present average data if the standard deviation for the mean field value at each location were reduced by a factor of about 5. To achieve this with the present instrumentation might be done by increasing the number of response epochs recorded at each measurement position by a factor of 25. However, this was considered to be too stressful for a subject and therefore was not attempted.

Now we turn to the recent results of our collaboration with the group at HUT. Responses

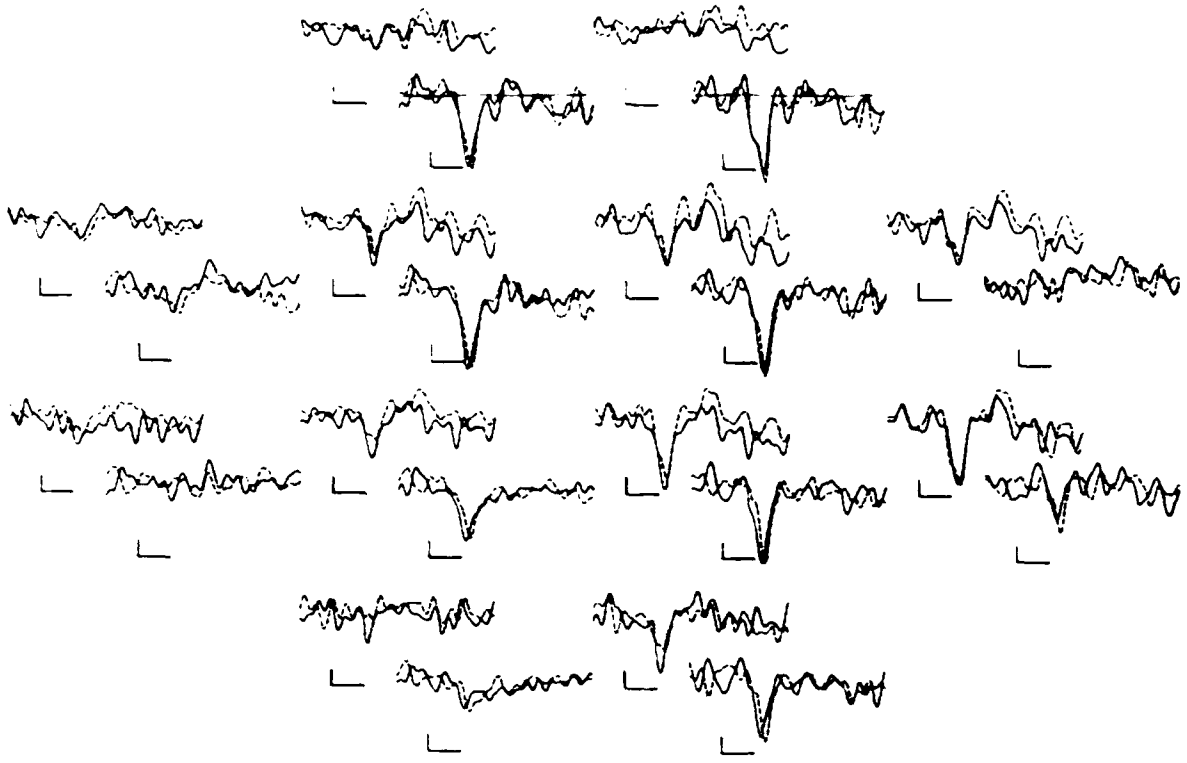

Figure 23: Responses to luminance stimuli obtained with the 24-sensor system at HUT. The upper-left set of traces for each position represent the field gradient along the upward (y) direction, and the lower-right set indicate the field gradient along the rightward (x) direction. Dashed lines show responses to a grating of 12 c/deg spatial frequency, and solid lines show responses to appearance of a solid circle.

of the second set of measurements are shown in Fig. 23 and Fig. 24. These illustrate the averaged responses obtained over the occipital area of one subject with an array of planar gradiometers that records data simultaneously at 12 positions over the scalp. There are two sets of data for each position, and each set consists of the average response (solid line) for a stimulus filling a circle and the average response (dashed line) for a grating pattern. The two sets indicate the time-course of the signals sensed by two orthogonally oriented gradiometers: The upper left set indicates responses provided by a sensor monitoring the gradiant of the radial field with respect to the x-direction across the array. The second set just to the lower right of the first set indicates responses provided by a sensor monitoring the gradient of the radial field with respect to the y-direction across the array. The x and y axes are oriented so that the y axis is approximately parallel to the midline of the scalp.

Comparing the offset between the strong negative peaks of solid and dashed curves indicates that the latency for the grating stimulus is markedly longer than for the circle stimulus when a chrominance stimulus is employed. Moreover, for both grating and circle the latency for chrominance responses is longer than for luminance responses.

However, careful inspection of the field patterns indicated by the data for chrominance

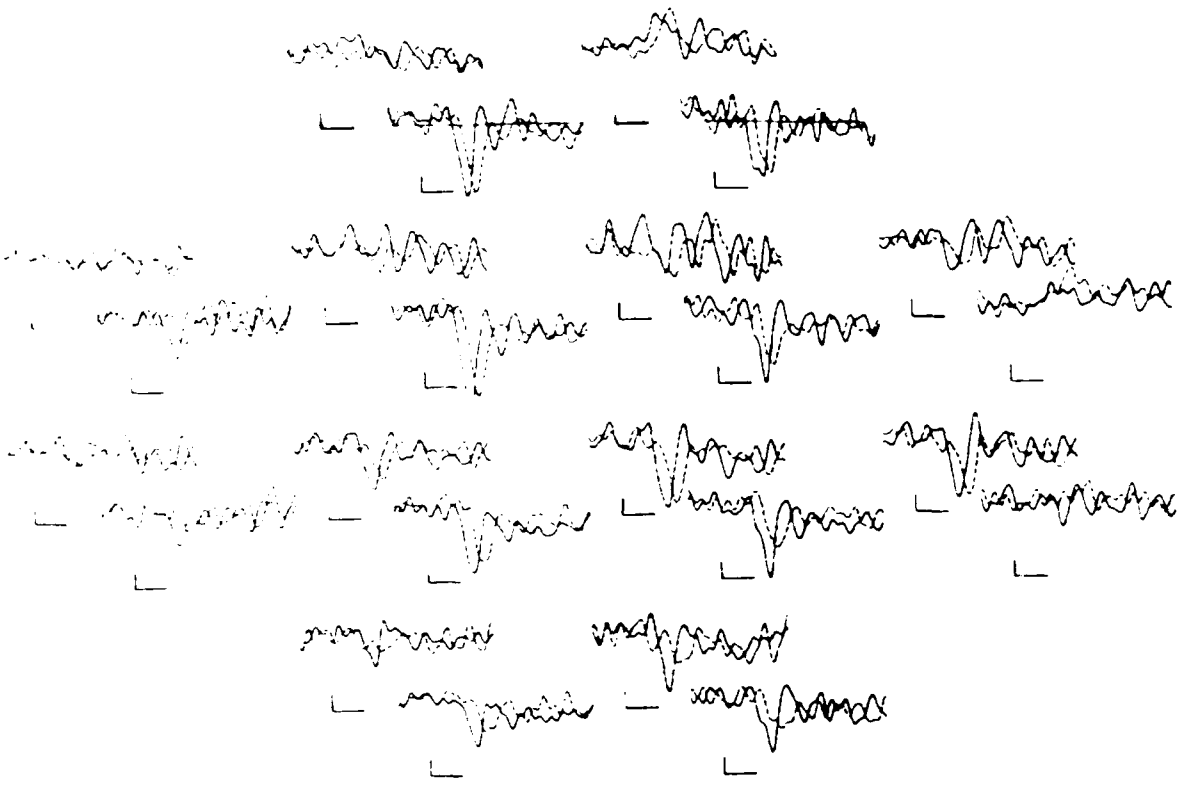

Figure 24: Responses to chrominance stimuli obtained with the 24-sensor system at HUT, with dashed lines showing responses to a grating of 12 c/deg spatial frequency and solid lines showing responses to appearance of a red circle on a green background at constant luminance.

and luminance stimuli fail to reveal any significant differences in location of the responding neuronal activity. Stimulus size was found to be insignificant. In fact, whether the condition was "red-on-green", "Mondrian", "gratings", or a "subtraction" mode, there was no discernible divergence in the locations of chrominance and luminance responses.

5.2.2 Summary

Initial studies at NYU revealed three response components at latencies of about 80, 150, and 220 ms for *rg* stimuli presented in the lower left quadrant of the visual field. more rostral than the other. This suggests that the underlying source current is oriented nearly perpendicular to the midline, as would be expected if the active area lies mostly along the cortical layer forming the left wall of longitudinal fissure, perhaps including adjacent areas of exposed cortex. Activity along the left wall is consistent with a source in area 17, although the cruciform model would predict activity along the ceiling of the left calcarine fissure as well. Maier et al. [63] conclude from a principal component analysis of VEP data for a monochromatic stimulus that the CI component (Jeffreys and Axford notation [37, 38]) with a latency of about 80 ms arises from cortical area 18 or possibly 19 (see also

Drasdo [20]), whereas the CII component with 120 ms latency originates in area 17. Recent electrophysiological studies of cat visual cortex provide evidence that feedback from V2 to the upper cortical layer of V1 can elicit strong activity, a feature that would be consistent with the findings just mentioned. The CIII component of 220 ms latency is more lateral to CII and therefore likely originates in area 18 or 19 as well. In the present studies, there is no evidence for a downward shift between the current dipole representing the neuronal source for 80 ms and that for the 120 ms components, as might be expected if they were to arise in area 18 and 17 respectively. However, there is a tendancy for the 220 ms source to lie more lateral than the others. There was no significant difference in the field patterns for *rg* and *bw* stimuli for all three components in both subjects.

Nonetheless, our thorough neuromagnetic measurements across the scalp where magnetic fields of activity in visual cortex should appear did not find differences in locations of neural activity in responses to chrominance and luminance stimuli. None of the cortical areas that are candidates for sources of the three components observed in this study can be identified as V4. It may well be that the cortical area where chrominance information is disassociated from luminance is located too far from the midline for detection in the present studies. The possibility remains, however, that extending these measurements to the temporal area may well reveal relevant activity in the temporal lobe.

6 "Latent" Sources of Auditory Cortical Activity

During the past year we undertook a research program to investigate the possibility that sensory evoked activity may reveal certain characteristics related to short term memory. We chose the auditory system for this search, since primary and secondary cortical areas are relatively compact. This feature is an advantage, because a fairly comprehensive survey could be made by confining measurements to a comparatively small area of the scalp. Moreover, a wider repetoire of stimuli could be provided than for the somatosensory system, which is also relatively compact. Unlike for vision, extracranial measurements of auditory-evoked scalp potentials track activity from brainstem to primary and association areas. Six major components can be observed in scalp potentials from the brainstem within the first 10 ms following a click stimulus [39], and anomalies in timing and strength have been correlated with specific disease states [109]. Some of the locations of brain-stem sources can be inferred from scalp potential measurements [101]. Middle latency components have recently received attention, since they can be observed both electrically and magnetically [98]. A sequence with latencies of 19, 30, and 50 ms commences with activity in the depth of the lateral sulcus on the mesial portion of the supratemporal surface. Our group was first to point out that functional maps could be identified across the primary auditory cortex: The 50 ms component produced by a steady-state stimulus is tonotopically represented across the supratemporal plane, following a logarithmic progress [94] [95]. Extensive studies of the functional organization of the auditory cortex have since been carried out by several groups, and some examples are given by Hari and Lounasmaa [27].

The late components are particularly interesting for their association with cognitive functions. The most prominent is N100, a peak that produces a negative potential at the vertex relative to a mastoid reference, with a latency of about 100 ms after onset of an auditory stimulus. Studies in our laboratory demonstrated that it is affected by by whether or not the

subject is paying attention to the stimulus [17]. The N100 component has been the object of intense study, for its amplitude is strongly affected by an number of cognitive factors [31] [86] [103] [104] [105] [2]. The N100 is followed by the P200 which peaks at about 180 ms. Responses to a stimulus that deviates in frequency for a series of stimuli of a given tone produce a larger N100 and smaller P200. The difference between this response to a deviant and the response to the standard is called the "mismatch negativity" (MMN), which produces a peak in the range 150 - 200 ms whether or not the subject pays attention to the stimuli.

Many additional features of these long-latency auditory components have recently been discussed by Scherg, Vajsar and Picton [99]. In fact, Näätänen and Picton [74] suggest that as many as 6 different "components" of the N100 may be affected in greater or lesser degree by acoustic stimulation, depending upon the attentiveness of the subject, and possibly other processes as well. These components are:

(1) Activity generated in primary auditory cortex.

(2) Responses generated in association area on the lateral surface of temporal and parietal cortex. This may well produce the T-complex of Wolpaw and Penry that occurs about 30 ms later than the vertex N100 [122]. They reported a positive peak at 105 ms (called Ta) and a negative peak at 155 ms (Tb) overlapping a separately generated vertex N100-P200 response, the latter now attributed to activity in primary auditory cortex; Celesia recorded on the lateral surface of temporal lobe and found similar components [9]. Other papers report a temporal 140 ms component that is similar to the Tb wave [65] [64] [87] [85] [84] [123]. Most papers suggest the latter component results from a radially oriented dipole in the temporal lobe.

(3) Motor and premotor cortices may contribute to N100 as well, but the evidence is scant.

(4) The mismatch negativity MMN may contribute additively to N100. The source of the MMN has recently been determined magnetically by Sams et al. (in press) to lie within about 1 cm of the source of N100 in the supratemporal plane. Näätänen suggested that MMN signals the existence of a precise, rapidly decaying and automatic neuronal representation of the physical features of a stimulus [73] and that it may form the basis of auditory sensory or "echoic" memory [75].

(5) A temporal source is associated with the processing negativity. This baseline shift is sometimes referred to as the negativity difference (Nd) wave, and it is presumed to contribute additively to N100.

(6) A frontal component is also identified with the processing negativity and Picton (1974) suggests that it reflects short-term memory processes.

The first three of the above six components are controlled by the physical and temporal aspects of the stimulus and by the general state of the subject; whereas the latter three are not necessarily evoked by a stimulus but depend on the conditions in which the stimulus occurs, i.e., they are endogenous components. These often are sustained much longer than the first three components, which they overlap in time. Näätänen has suggested (personal communication) there may well be an additional component generated by a radial source somewhere near the vertex to account for the continued enhancement with ISI seen in the scalp recorded EEG.

The mismatch negativity of Näätänen may contribute to N100 if not specifically separated out, as can the similar negativity difference Nd of Hillyard, which is affected by attention

but may shift in phase with respect to N100, depending upon the nature of the task. Thus, the most widely held view is that many different areas of the brain contribute to the N100 detected at the vertex in the EEG. The weights given to these various components depend upon the kind of mental process in which the subject is engaged.

In contrast with this, the magnetic counterpart to N100 (denoted N100m) has, up to now, been thought to be fully accounted for by activity of auditory cortex. The place of the maximum neuronal activity along the tonotopic axis is reported to relate to the pitch of a sound tone (corresponding to the location of the fundamental frequency in a missing fundamental paradigm) [79]. Its location on cortex may also be affected by its loudness, with activity shifting anterior for louder tones along a direction that is approximately orthogonal to the tonotopic locus [33]. Recently, evidence has been presented that N100m may actually represent a neuronal excitation whose center of activity shifts across the cortical surface during its period of activity [92].

The most convincing piece of evidence to date for multiple contributions to N100 was provided by Hari et al. [29] who studied the increase in N100m and N100 response strengths with increasing interstimulus interval (ISI). Tone bursts with ISI ranging from 1 to 16 s were employed. Recordings were made of both N100 via scalp electrodes along the midline and N100m by a sensor placed over the right parietal scalp. It was centered approximately over a field extremum of N100m, where the field is known to enter the scalp and to have its maximum radial value. The amplitude of the electrical N100 recorded at the vertex was found to increase monotonically with ISI up to 16 s, while the latency increased by 20 ms [112]. However, the amplitude of N100m increased with ISI only up to 4 s, becoming independent of ISI for longer intervals, and there was no evident change in latency. Therefore, Hari et al. concluded that the source of N100m was not identical to that of N100. While all measurements of N100m were restricted to the right hemisphere, but the N100 recorded at the vertex "saw" the superimposed response of both hemispheres, the possibility that the difference could be due to asymmetrical hemispheric responses was not entertained.

Scherg and von Cramon [102] [100] formalized a widely espoused "explanation" of the difference found by Hari and her colleagues between electric and magnetic recordings. They proposed a model in which a radially oriented dipole lying on the exposed cortical surface below the supratemporal plane contributes to the EEG at the vertex but is also invisible to the MEG. This is possible in principle, since a radially oriented dipole in a spherical head would be "magnetically silent". However, in view of recent estimates developed in this laboratory [61] (reported in our previous Annual Report) for the spatial extent of cortical activity contributing to components of the EEG and MEG, it is unlikely that such cortical activity is completely radial. For example, an area of about 200 mm^2 would be required to account for the deduced neuronal strength of the N100m component. Because of the convoluted topology of the cortical surface, it is likely that there is a tangential component of this "radial" source and that it may be detected magnetically.

Indeed, studies begun this year in our laboratory suggest that this latter point is worth pursuing. We now report the first evidence for an additional neuronal source that is active simultaneously with the magnetically detected N100m and a second source that coincides with P200m. Of particular interest is the feature that these neuronal sources exhibit quite different functional characteristics than N100m and P200m.

6.1 Studies of the Latent Components

Three subjects were presented with a series of tone bursts to the left ear, and the neuromagnetic field was recorded over the lateral area of the right hemisphere. The tone duration was 500 ms, with linear rise and fall times of 10 ms duration to enhance spectral purity. Aside from the classic N100m and P200m, no detectible response was found for an interstimulus interval (ISI) of 1 s. However, when measuring over a region of the lateral scalp where the classic N100m is not detected, an ISI of 2 s produced a weak response that emerged from the noise, and this component became quite robust for an ISI of 4 s. As shown in Figure 25, it is a monophasic component that peaks at about 80 ms following onset of the burst. This latency is identical to that of N100m for this subject and stimulus conditions. This component continues to grow in strength with ISI, at least to ISI = 8 s. It can be detected only if there has been no immediately preceding tone of similar frequency. However, a tone of 9 kHz presented 1 s before has no effect on its amplitude. We emphasize that this component cannot be detected in our studies when stimuli are presented at conventional rates with ISIs of about 1 s or less. Hence the neuronal generator(s) of this new component cannot be the same as those that underly the conventionally measured N100m.

In addition to this 80-ms component, Figure 25 shows that a second component of opposite polarity appears when the ISI is longer than about 6 s. Its early stage may temporally overlap the last stage of the preceding 80-ms component, but it establishes its own identity at a latency of about 150 ms and reaches its peak at 170 ms. This latency coincides with that of the classic P200m for this subject.

Similar behavior for the 80-ms and 150-ms components that appear at long ISI has been found in two other subjects. For convenience, we shall denote these two new components as the *latent components*, a terminology based on the dictionary definition of *latent* as "Not visible or apparent but capable of developing or being expressed". Therefore, we shall provisionally denote the first component by the symbol "L80m" and the second by the symbol "L170m".

In addition to its strong dependency on ISI, the position of at least one field extremum distinguishes L80m and L170m from the well-known N100m and P200m elicited by a train of identical tone bursts [24] [28] [100]. The absence of the classic auditory evoked components (e.g, P50m, N100m, and P180m components) at the scalp positions where the recordings of Figure 25 were made for short ISI is especially convincing evidence that the neuronal sources of both latent signals are spatially displaced from each other.

It has long been known that the classic N100 and P200 components exhibit refractory properties, so that amplitudes diminish if a stimulus is presented sufficiently soon after an identical one [18], and this effect may persist for as long as 10 s [7] [76] [68] [88]. However, these refractory effects are not as dramatic as those illustrated in Figure 25 for ISIs of 1 and 2 s. None of the six candidates described by Näätänen and Picton appear to match the L80m and L170m components revealed in this figure. The one closest in latency to L170m (Tb of Wolpaw and Penry) is apparently oriented radially, whereas L170m clearly has a strong tangential component.

We may consider two other components that are clearly endogenous: the well-known N200 and P300 components. Only N200 has a latency that approximates that of one of our latent components, the L170m. Perhaps the most important distinction between the

(a) ISI = 1 s

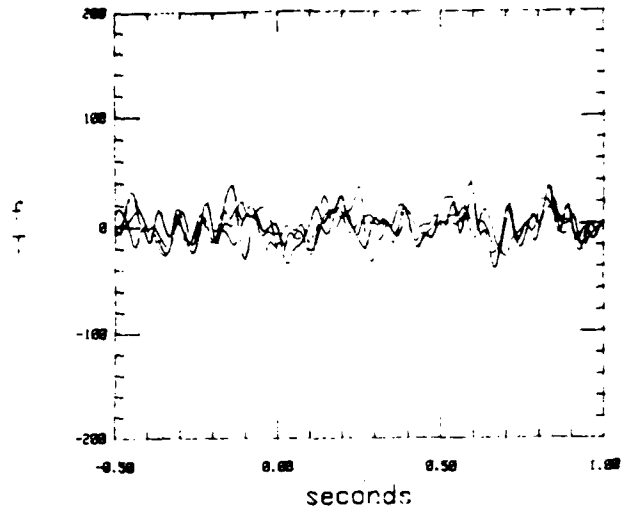

(b) ISI = 2 s

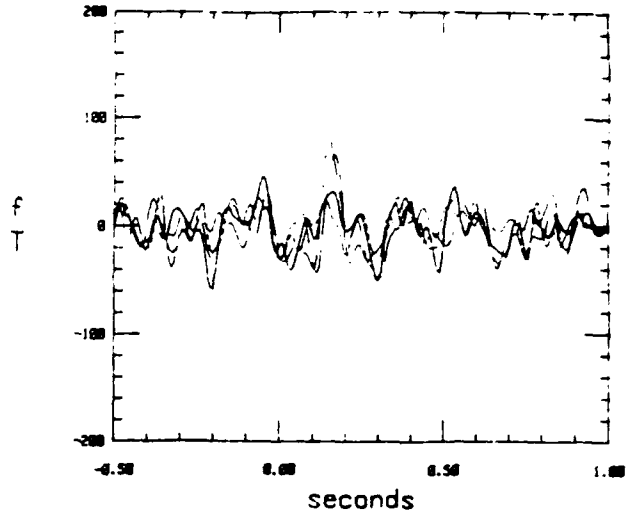

(c) ISI = 4 s

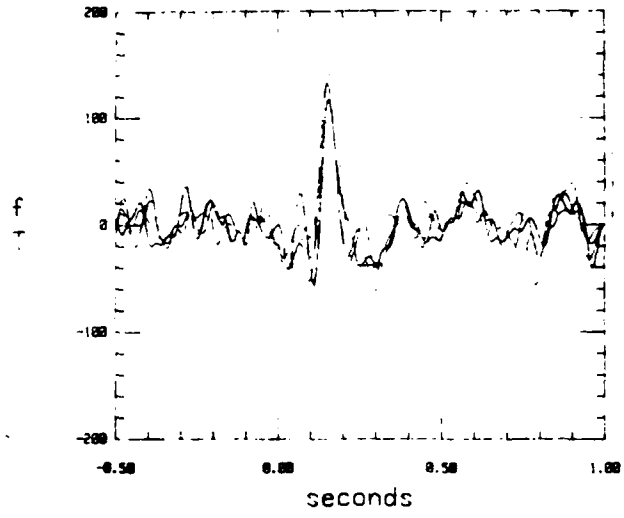

(d) ISI = 8 s

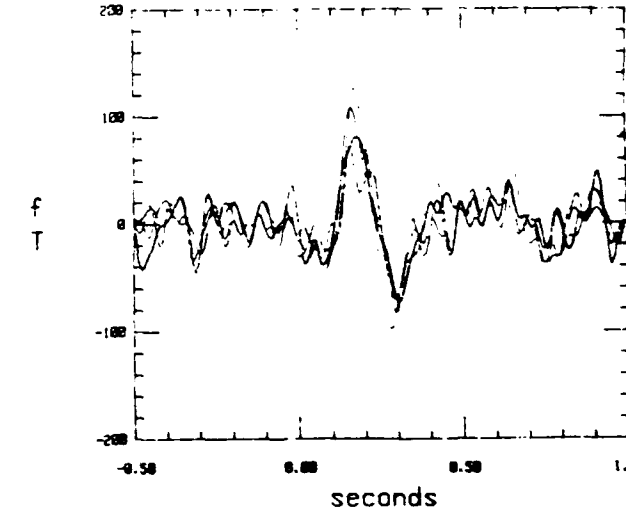

Figure 25: Observed latent components over the right hemisphere averaged for 100 epochs, with signals from 4 MEG channels shown. Data were bandpassed in the range 1 - 50 Hz. Stimulus onset was at 100 ms.

L170m component in our pilot study and the classic N200 and P300 is the orientation of the neuronal current that corresponds to the field pattern. The latter is directed upward toward the region of scalp between parietal and occipital areas, but L170m has quite a different orientation.

Owing to their dependency on ISI and the fact that the time intervals involved are on the order of seconds rather than milliseconds, it seems quite likely that these latent components reflect cognitive functions. Of course, at this stage of our investigations we may only offer conjectures, and these will form the basis for our experiments in the coming year. As a working hypothesis we suggest that the latent components may reflect a memory function, although at this stage we cannot discount the possibility they signal an attentional or (less likely) variation in arousal level associated with time to the next stimulus.

In this regard, we should consider the known forms of memory in humans which are commonly classified as: ectopic, echoic, short-term, and long-term. The first two are sometimes referred to as "sensory memory" components because they emphasize the physical characteristics of the stimulus. Ectopic has the shortest retention time, lasting for only a few hundred milliseconds, and is not relevant to the latent components. However, echoic memory, which may persist for as long as 10 s and records the physical features of the acoustic stimulus, is of considerable interest. Because of its relatively long duration, echoic store is probably a function of sensory cortex. Similarly, short-term memory records the content of a stimulus for minutes, but since it is still modality-specific [72] operations related to its use are undoubtedly reflected in activity of neocortex, perhaps including association areas as well as sensory projection areas.

In contrast with short-term memory, long-term memory can retain information indefinitely and it is material-specific rather than modality-specific. However, there is evidence that long-term memory can contain information about voice characteristics [14]. Neocortex is certainly involved in retrieving long-term memories, but the locus involved is dependent more on the nature of the materials, e.g., verbal versus pictorial, regardless of the modality of presentation of stimuli in a particular experiment.

Naturally, within all of these categories of memory there are subcategories, e.g., memory for episodes and objects and memory for procedures (skill). The amygdala is involved in memories with emotional content, [50] and hippocampus with processing declarative or episodic information [126]. So any study of brain activity related to memory must be quite specific as to the categories and subcategories involved, as different types of memory may involve very different brain processes and locations.

A recent study of auditory short-term memory in monkeys illustrates that sensory association cortex plays an essential role. Monkeys were trained to perform auditory and visual short-term memory tasks with a delayed matching-to-sample paradigm [11]. Following a 20 s inter-trial interval, a high tone or low tone was presented by a speaker to the right of the monkey. The monkey indicated it was heard by pressing a lever under the speaker, and this terminated the tone and initiated a delay interval. Then the comparison tone was presented by a speaker on the left, and if it matched the first and the monkey responded sufficiently quickly by pressing a lever under this speaker, he was rewarded. If it did not match and the monkey correctly withheld response, there was no reward. If the monkey made an incorrect response, he was punished by extinguishing the lights within the chamber for 60 s. Achievement performance that was typically 95% - 100% for a delay of 0.5 s or 4 s decreased

to about 80% for a delay of 32 s, A comparable visual memory task was also performed as a control.

On completion of training and testing, three monkeys received unilateral ablations of their auditory association cortex (cytoarchitectonic area TA of von Bonin and Bailey [113] [114]), sparing primary area (TC). This included the lateral surface of the superior temporal sulcus and the upper bank of the superior temporal sulcus. Visual discrimination was completely unaffected by unilateral lesions. All three monkeys showed temporary impairment for auditory discrimination, but with training two of them achieved performance at the preoperative level. The third was able to achieve only 87% at 0.5 s delay and about 70% at 32 s delay even after training for 3 months. Following a second operation in which ablation was carried out for the second hemisphere, severe impairments in short-term memory were observed. The fact that visual discrimination performance remained intact ruled out any motivational impairment as the basis for the auditory deficits. Failure of tone discrimination can be ruled out as an explanation, because monkeys retained ability to discriminate tones separated by 1 octave in the low frequency range and by less than an octave in the high frequency range, whereas the high-frequency and low-frequency tones in the experiments were separated by almost 4 octaves, thereby making them easily discriminable.

6.2 Human Sensory Memory Store

Numerous studies provide evidence for two phases of auditory sensory storage: an intial phase lasting several hundred milliseconds in which there is an unanalyzed trace of the stimulus, and a second phase lasting several seconds in which there is partly analyzed information, such as coded speech features. The latter is characterized by most measures of echoic memory. We suggest that L80m or L170m, or both, may be involved in echoic storage primarily because of the long ISI of several seconds that is required to gain full expression of their amplitudes is comparable to time constants of about 4 - 10 s revealed by psychophysical studies of echoic memory. In this sense, the response strength may well represent reinforcement, or reactivation, of memory store. This is comparable to characteristic times revealed in studies of short-term memory when freely recalling the items on the list [25]. There is marked deterioration in performance for the last three if a delay of as little as 10 s is imposed before the recall: Recall accuracy becomes equal to those in the middle of the list, implying that short-term store is largely lost over a time interval of about 10 s.

Studies are presently underway to address the possiblity that L80m and/or L170m play roles in echoic, and perhaps short-term memory store, that are quite distinct from the role that P300 is believed to play in declarative memory. The latter may well signal the transfer of information from sensory memory store to long-term store in extrasensory areas, where the transfer is mediated by activity in the hippocampus. One of the objectives of this proposed research is to determine whether activity signaled by the latent components is not only stimulus-specific but also to a degree content specific. Following the suggestion of Cowan [13], we may accept the working hypothesis that short-term storage may be considered as the sum of all "activated" information. If a novel stimulus is presented, its relevant memory elements are "activated" (stored) in echoic store. As mentioned, an increase in response strength with ISI displayed by the latent components may reflect the process of activating stimulus information in memory, or of reinforcing that information in memory. Should an

identical stimulus be presented after this store is partically degraded, the latent components may well signal the re-activation. We note that this occurs simultaneously with processing in sensory cortex, as indicated by the coincidence of the latencies for N100m and L80m, as well as for P200m and L170m. If the stimulus is novel, full activation is required, thereby producing the strongest amplitude for the latent components. An investigation of how these concepts relate to the properties of the latent components must await further studies.

7 Personnel

The following personnel participated in portions of the research described in this Report.

Faculty

Dr. Lloyd Kaufman, Professor of Psychology and Center for Neural Science, Adjunct Professor of Physiology and Biophysics.

Dr. Samuel J. Williamson, University Professor, Professor of Physics and Neural Science, Adjunct Professor of Physiology and Biophysics

Research Staff

Dr. Sarah Curtis, Associate Research Scientist

Dr. Jia-Zhu Wang, Associate Research Scientist

Dr. Carlo Salustri, Visiting Scholar

Graduate Students

Yael Cycowicz (Department of Psychology)

Gladys Klemic (Department of Physics)

Zhonglin Lü (Department of Physics)

Lian Tao (Department of Physics)

Undergraduate Student

Robert Kalimi (Department of Biology), B.A. Honors Thesis

High School Student

Michael Gat (Westinghouse Science Talent Search Semi-Finalist)

Administrative Secretary

Wei Sun

8 Invited Talks given by Members of the Laboratory

29 March, *Neuromagnetism*, Colloquium, Department of Physics, Polytechnic University, Brooklyn.

31 March, *Magnetic Characterization of Brain Function – Epilepsy Today, Alzheimer's and Sechzophrenia Tomorrow*, Plenary Session, Medical Alumni Day, New York University School of Medicine.

20 April, *Advances in Superconducting Biomagnetic Instrumentation*, Seminar, Superconducting Technology, Inc., Santa Barbara, California.

21 April, *Bioelectricity and Biomagnetism in the Central Nervous System*, Workshop on Bioelectricity and Biomagnetism in Clinical Medicine: What is it, Where is it going, is it practical and affordable?, Little Company of Mary Hospital, Torrance, California.

4 May, *Neuromagnetic Localization of Sensory and Cognitive Functions*, Third Swiss EEG-EP Mapping Meeting, Department of Neurology, University Hospital, Zürich, Switzerland.

23 May, *Neuromagnetism: A Bridge that Physics Provides between Physiology and Cognition*, Seminar, Department of Physics, Universidade de Lisboa, Portugal.

1 June, *Recent Advances in Neuromagnetism*, Seminar, Center for Neuromagnetism, Veterans Administration Hospital, Albuquerque, New Mexico.

4 June, *Advances in Cognitive Studies with Neuromagnetic Techniques*, Seminar, Neuromagnetism Laboratory, Life Sciences Division, Los Alamos National Laboratory, Los Alamos, New Mexico.

7 September, *Magnetic Investigations of Higher Levels of Brain Function*, Colloquium, Department of Electronics, Kyushu University, Fukuoka, Japan.

13 September, *Evolution of Neuromagnetic Topographic Mapping*, Invited Special Lecture, First International Congress on Brain Electromagnetic Topography, Osaka, Japan.

26 September, *Principles of Neuromagnetism*, Course on Magnetism in Clinical Neurophysiology, Annual Meeting of the American Electroencephalographic Society, Houston, Texas.

10 October, *Neuromagnetism: A Bridge between Physiology and Cognition*, Colloquium, Department of Physics and Astronomy, Rutgers the State University of New Jersey, Piscataway, New Jersey.

12 October, *Magnetic Source Imaging: Capabilities and Prospects for Neuromagnetism*, Seminar, Mayo Clinic, Rochester, Minnesota.

16 November, *Neuromagnetic Insight into Human Brain Functions from Physiology to Cognition*, Seminar, Department of Physiology and Biophysics, University of Washington, Seattle, Washington.

17 November, *Magnetic Methods for Determining the Functional Organization of Human Auditory Cortex*, Special Invited Talk, American Speech-Language-Hearing Association 1990 Annual Convention, Seattle, Washington.

30 November, *Neuromagnetic Studies of Human Sensory and Cognitive Brain Functions*, Colloquium, Department of Physics, Columbia University, New York City.

5 December, *Parallels in the Functional Organization of Sensory Cortex: Humans and Animals*, Seminar, Institute of Animal Behavior, Rutgers the State University of New Jersey, Newark, New Jersey.

19 December, *Neuromagnetic Studies of the Human Brain with SQUID Sensors: From Physiology to Cognition*, Seminar, Medical Research Department, Brookhaven National Laboratory, Upton, New York.

8 February, 1991, *Magnetic Techniques for Mapping Spatial Organization of Sensory and Cognitive Functions of the Human Brain*, Recent Advances in Neuroscience at New York University, Sumposium in association with the Fidia Foundation exhibit "The Enchanted Loom: The Discovery of the Brain", New York University Medical Center.

9 Publications from the Neuromagnetism Laboratory

9.1 Publications Recently Appearing

L. Kaufman and S. J. Williamson. Neuromagnetic localization of neuronal activity in visual and extra-visual cortex. In B. Cohen, editor, *Vision and the Brain*, pages 271–287, Raven Press, New York, 1990.

S. J. Williamson and L. Kaufman. Theory of neuroelectric and neuromagnetic fields. In F. Grandori, H. Hoke, and G. L. Romani, editors, *Auditory Evoked Magnetic Fields and Electric Potentials*, pages 1–39, Karger, Basel, 1990.

L. Kaufman and S. J. Williamson. Responses to steady-state auditory stimulation. In F. Grandori, H. Hoke, and G. L. Romani, editors, *Auditory Evoked Magnetic Fields and Electric Potentials*, pages 283–312, Karger, Basel, 1990.

L. Kaufman, B. Schwartz, C. Salustri, and S.J. Williamson. Modulation of spontaneous brain activity during mental imagery. *J. Cognitive Neuroscience*, 2:124–132, 1990.

S.J. Williamson and L. Kaufman. Seeing neuromagnetically. *Arkhimedes*, 42:211–227, 1990.

9.2 Articles in Press

Z. Lü and S.J. Williamson. Spatial extent of coherent sensory-evoked cortical activity. *Exp. Brain Res.*, in press, 1991.

L. Kaufman, J. Kaufman, and J.Z. Wang. On cortical folds and neuromagnetic fields. *Electroenceph. Clin. Neurophysiol.*, in press, 1991.

9.3 Manuscripts Submitted

L. Kaufman, Y. Cycowicz, M. Glanzer, and S. J. Williamson. Selective suppression of spontaneous cortical rhythms for cognitive tasks of imaging and rhyming. submitted, 1991.

L. Kaufman, S. Curtis, J.Z. Wang, and S.J. Williamson. Changes in cortical activity when subjects scan memory for tones. submitted, 1991.

L. Kaufman, S. Curtis, J.-Z. Wang, and S.J. Williamson. Changes in cortical activity when subjects scan memory for tones. In *8th International Conference on Biomagnetism*, 1991.

Z.-L. Lü, J-Z. Wang, and S.J. Williamson. Neuronal sources of human parieto-occipital alpha rhythm. In *8th International Conference on Biomagnetism*, 1991.

J-Z. Wang, L. Kaufman, and J.H. Kaufman. Simulation of activity of visual cortex. In *8th International Conference on Biomagnetism*, 1991.

References

[1] P. Andersen and S. A. Andersson. *Physiological Basis of the Alpha Rhythm.* Appleton-Century-Crofts, New York, 1968.

[2] D. Arthur, S. Hillyard, E. Flynn, and A. Schmidt. Neural mechanisms of selective auditory attention. In S. J. Williamson, M. Hoke, G. Stroink, and M. Kotani, editors, *Advances in Biomagnetism*, pages 113–116, Plenum, New York, 1989.

[3] D. S. Barth and W. Sutherling. Current source-density and neuromagnetic analysis of the direct cortical response in rat cortex. *Brain Res.*, 450:280–294, 1988.

[4] H. Berger. Uber das Elektroenkephalogramm des Menschen. II. *J. Psychol. Neurol. (Lpz.)*, 40:160–179, 1930.

[5] P.W. Brazis, J.B. Biller, and M. Fine. Central achromatopsia. *Neurology*, 31:920, 1981.

[6] D. S. Buchanan. Impact of different noise sources on dipole localization in the spherical model: A simulation. In S. J. Williamson, M. Hoke, G. Stroink, and M. Kotani, editors, *Advances in Biomagnetism*, pages 539–542, Plenum, New York, 1989.

[7] R. A. Butler. Effect of changes in stimulus frequency and intensity on habituation of the human vertex potential. *J. Acoust. Soc. Am.*, 44:945–950, 1968.

[8] L.J. Cauller and A.T. Kulics. The neural basis of the behaviorally relevant N1 component of the somatosensory-evoked potential in SI cortex of awaked monkeys: evidence that backward cortical projections signal conscious touch sensation. *Exp. Brain Res.*, in press, 1991.

[9] G. G. Celesia. Organization of auditory cortical areas in man. *Brain Res.*, 99:403–414, 1976.

[10] M. Clynes and M. Kohn. Spatial VEPs as physiologic language elements for colour and field structure. *Electroenceph. Clin. Neurophysiol.*, 26 (Suppl. 1):82–96, 1967.

[11] M. Colombo, M.R. D'Amato, H.R. Rodman, and C.G. Gross. Auditory association cortex lesions impair auditory short-Term memory in monkeys. *Science*, 247:336–338, 1990.

[12] P. Costa Ribeiro, S. J. Williamson, and L. Kaufman. SQUID arrays for simultaneous magnetic measurements: Calibration and source localization performance. *IEEE Trans. Biomed. Engr.*, BME-35:551–560, 1988.

[13] N. Cowan. Evolving conceptions of memory storage, selective attention, and their mutual constraints within the human information-processing system. *Psych. Bull.*, 104:163–191, 1988.

[14] N. Cowan. On short and long auditory stores. *Psych. Bull.*, 96:341–370, 1984.

[15] O.D. Creutzfeldt. The neocortical link: thoughts on the generality of structure and function of the neocortex. In M.A.B. Brazier and H. Petsche, editors, *Architectonics of the Cerebral Cortex, IBRO Monograph Series*, pages 357–384, Raven Press, New York, 1978.

[16] S. Curtis, L. Kaufman, and S. J. Williamson. Divided attention revisited: Selection based on location or pitch. In K. Atsumi, M. Kotani, S. Ueno, T. Katila, and S. J. Williamson, editors, *Biomagnetism '87*, pages 138–141, Tokyo Denki University Press, Tokyo, 1988.

[17] S. Curtis, L. Kaufman, and S.J. Williamson. Attention modulates N1 and P2 components of auditory cortex. In preparation, 1990.

[18] H. Davis, T. Mast, N. Yoshie, and S. Zerlin. The slow response of the human cortex to auditory stimuli: Recovery process. *Electroenceph. Clin. Neurophysiol.*, 21:105–113, 1966.

[19] A. M. Derrington, J. Krauskopf, and P. Lennie. Chromatic mechanisms in lateral geniculate nucleus of macaque. *J. Physiol.*, 357:241–256, 1984.

[20] C. Barber, editor. *Cortical Potentials Evoked by Pattern Presentation in the Foveal Region*. MTP Press, Lancaster, 1980.

[21] E. Ducla-Soares, D. Rose, and S. Sato. Volume current effects in magnetoencephalography. *Phys. Med. Bio.*, 33:suppl. 1, 1988.

[22] F. Duffy. Clinical use of brain electrical activity mapping. In G. Pfurtscheller and F.H. Lopes da Silva, editors, *Functional Brain Imaging*, pages 149–160, Hans Huber Publishers, Toronto, 1988.

[23] F. H. Duffy. *Topographic Mapping of Brain Electrical Activity*. Butterworths, Stoneham, MA, 1986.

[24] C. Elberling, C. Bak, B. Kofoed, J. Lebech, and K. Særmark. Magnetic auditory responses from the human brain: A preliminary report. *Scand. Audiol.*, 9:185–190, 1980.

[25] M. Glanzer and A.R. Cunitz. Two storage mechanisms in free recall. *J. Verbal Learning and Verbal Behavior*, 5:351–360, 1966.

[26] M. S. Hämäläinen and J. Sarvas. Feasibility of the homogeneous head model in the interpretation of neuromagnetic fields. *Phys. Med. Biol.*, 32:91–97, 1987.

[27] R. Hari. Activation of the human auditory cortex by various sound sequences: Neuromagnetic studies. In S. J. Williamson, M. Hoke, G. Stroink, and M. Kotani, editors, *Advances in Biomagnetism*, pages 87–92, Plenum, New York, 1989.

[28] R. Hari, K. Aittoniemi, M.-L. Järvinen, T. Katila, and T. Varpula. Auditory evoked transient and sustained magnetic fields of the human brain: Localizaton of neural generators. *Exp. Brain Res.*, 40:237–240, 1980.

[29] R. Hari, K. Kaila, T. Katila, T. Tuomisto, and T. Varpula. Interstimulus interval dependence of the auditory vertex response and its magnetic counterpart: Implications for their neural generation. *Electroenceph. Clin. Neurophysiol.*, 54:561–569, 1982.

[30] M.J. Hawken, A.J. Parker, and J.S. Lund. Laminar organization and contrast sensitivity of direction-selective cells in the striate cortex of the Old-World monkey. *J. Neurosci.*, 8:3541–3548, 1988.

[31] S. A. Hillyard, R. F. Hink, V. L. Schwent, and T. W. Picton. Electrical signs of selective attention in the human brain. *Science*, 182:177–180, 1973.

[32] J.A. Hobson and M. Steriade. Neuronal basis of behavioral state control. In V.B. Mountcastle, F. Bloom, and S.R. Geiger, editors, *The Nervous System: Handbook of Physiology*, pages 701–823, American Physiological Society, Bethesda, MD, 1986.

[33] M. Hoke, C. Pantev, K. Lehnertz, and B. Lütkenhöner. Tonotopic organization of the human auditory cortex revealed by transient auditory evoked magnetic fields. In K. Atsumi, M. Kotani, S. Ueno, T. Katila, and S. J. Williamson, editors, *Biomagnetism '87*, pages 142–145, Tokyo Denki University Press, Tokyo, 1988.

[34] J.-C. Huang, C. Nicholson, and Y. Okada. Distortion of magnetic evoked fields and surface potentials by conductivity differences at boundaries in brain tissue. *Biophys. J.*, 57:1155–1166, 1990.

[35] R. J. Ilmoniemi, S. J. Williamson, L. Kaufman, H.J. Weinberg, and A.D. Boyd. Method for locating a small magnetic object in the human body. *IEEE Trans. Biomed. Eng.*, 35:561–564, 1988.

[36] J.D. Jackson. *Classical Electrodynamics.* John Wiley & Sons, New York, 2nd edition, 1975.

[37] D. A. Jeffreys and J. G. Axford. Source locations of pattern-specific components of human visual evoked potentials. I. Component of striate cortical origin. *Exp. Brain Res.*, 16:1–21, 1972.

[38] D. A. Jeffreys and J. G. Axford. Source locations of pattern-specific components of human visual evoked potentials. II. Components of extrastriate cortical origin. *Exp. Brain Res.*, 16:22–40, 1972.

[39] D. L. Jewett and J. S. Williston. Auditory evoked far-fields averaged from the scalp of human. *Brain*, 94:681–696, 1971.

[40] M. Kajola, S. Ahlfors, G. J. Ehnholm, J. Hällström, M. S. Hämäläinen, R. J. Ilmoniemi, M. Kiviranta, J. Knuutila, O. V. Lounasmaa, C. D. Tesche, and V. Vilkman. A 24-channel magnetometer for brain research. In S. J. Williamson, M. Hoke, G. Stroink, and M. Kotani, editors, *Advances in Biomagnetism*, pages 673–679, Plenum, New York, 1989.

[41] L. Kaufman, M. Glanzer, Y. M. Cycowicz, and S. J. Williamson. Visualizing and rhyming cause differences in alpha suppression. In S. J. Williamson, M. Hoke, G. Stroink, and M. Kotani, editors, *Advances in Biomagnetism*, pages 241–244, Plenum, New York, 1989.

[42] L. Kaufman and Y. Locker. Sensory modulation of the EEG. 1970. 75th Meeting.

[43] L. Kaufman and R. Price. The detection of cortical spike activity at the human scalp. *IEEE Trans. Biomed. Eng.*, BME-14:84–90, 1967.

[44] L. Kaufman, B. Schwartz, C. Salustri, and S.J. Williamson. Modulation of spontaneous brain activity during mental imagery. *J. Cognitive Neuroscience*, 2:124–132, 1990.

[45] L. Kaufman and S. J. Williamson. Responses to steady-state auditory stimulation. In F. Grandori, H. Hoke, and G. L. Romani, editors, *Auditory Evoked Magnetic Fields and Electric Potentials*, pages 283–312, Karger, Basel, 1990.

[46] J. Knuutila, S. Ahlfors, A. Ahonen, J. Hällström, M. Kajola, O. V. Lounasmaa, V. Vilkman, and C. Tesche. Large-area low-noise seven-channel dc SQUID magnetometer for brain research. *Rev. Sci. Instrum.*, 58:2145–2156, 1987.

[47] J. Krauskopf, G. Klemic, O. V. Lounasmaa, D. Travis, L. Kaufman, and S. J. Williamson. Neuromagnetic measurements of visual responses to chromaticity and luminance. In S. J. Williamson, M. Hoke, G. Stroink, and M. Kotani, editors, *Advances in Biomagnetism*, pages 209–212, Plenum, New York, 1989.

[48] J. Krauskopf, D. R. Williams, and D. W. Heeley. Cardinal directions of color space. *Vison Res.*, 22:1123–1131, 1982.

[49] E.H. Land and J.J. McCann. Lightness and retinex theory. *J. Opt. Soc. Am.*, 61:1–11, 1971.

[50] J.E. LeDoux, A. Sakaguchi, and D.J. Reis. Subcortical efferent projections of the medial geniculate nucleus mediate emotional responses conditioned by acoustic stimulli. *J. Neurosci.*, 4:683–698, 1984.

[51] D. Lehmann. EEG assessment of brain activity: Spatial aspects, segmentation and imaging. *Int. J. Psychophysiol.*, 1:267–276, 1984.

[52] D. Lehmann, H. Ozaki, and I. Pal. Averaging of spectral power and phase via vector diagram best fits without reference electrode or reference channel. *Electroenceph. Clin. Neurophysiol.*, 64:350–363, 1986.

[53] P. Lennie, J. Krauskopf, and G. Sclar. Chromatic mechanisms in striate cortex of macaque. *J. Neurosci.*, 10:649–669, 1990.

[54] P. Lennie, C. Trevarthen, H. Waessle, and D.Van Essen. Parallel processing of visual information. In L. Spillman and J. Werner, editors, *Visual Perception: The Neurophysiological Foundations*, Academic, New York, 1989.

[55] M. Livingstone and D. Hubel. Segregation of form, color, movement, and depth: Anatomy, physiology, and perception. *Science*, 240:740–749, 1988.

[56] M. S. Livingstone and D. H. Hubel. Anatomy and physiology of a color system in primate visual cortex. *J. Neurosci.*, 4:309–356, 1984.

[57] M.S. Livingstone and D.H. Hubel. Psychophysical evidence for separate channels for the perception of form, color, motion, and depth. *J. Neurosci.*, 7:3416–3468, 1984.

[58] F. H. Lopes da Silva, T.H.M.T. van Lierop, C.F. Schrijer, and W. Storm van Leeuwen. Organization of thalamic and cortical alpha rhythms: Spectra and coherences. *Electroenceph. Clin. Neurophysiol.*, 35:627–639, 1973.

[59] F. H. Lopes da Silva, J. E. Vos, J. Mooibroek, and A. van Rotterdam. Relative contributions of intracortical and thalamo-cortical processess in the generation of alpha rhythms, revealed by partial coherence analysis. *Electroenceph. Clin. Neurophysiol.*, 50:449–456, 1980.

[60] F.H. Lopes da Silva and W. Storm van Leeuwen. The cortical alpha rhythm in dog: The depth and surface profile of phase. In M.A.B. Brazier and H. Petsche, editors, *Architectonics of the Cerebral Cortex*, pages 319–333, Raven Press, New York, 1978.

[61] Z. Lü and S.J. Williamson. Spatial extent of coherent sensory-evoked cortical activity. *Exp. Brain Res.*, in press, 1991.

[62] C.J. Lueck, S. Zeki, K.J. Friston, M.-P. Deiber, P. Cope, V.J. Cunningham, A.A. Lammertsma, C. Kennard, and R.S.J. Frackowiak. The colour centre in the cerebral cortex of man. *Nature*, 340:386–389, 1989.

[63] J. Maier, G. Dagnelie, H. Spekreijse, and B. W. Van Dijk. Principal components analysis for source localization of the VEP's in man. *Vis. Res.*, 27:165–177, 1987.

[64] W. C. McCallum and S. H. Curry. The form and distribution of auditory evoked potentials and CNV when stimuli and responses are lateralized. In H. H. Kornhuber and L. Deecke, editors, *Progress in Brain Research, Motivation, Motor and Sensory Processes of the Brain: Electrical Potentials*, pages 767–775, Elsevier, Amsterdam, 1980.

[65] W. C. McCallum and S. H. Curry. Hemisphere differences in event related potentials and CNVs associated with monaural stimuli and lateralized motor responses. In D. Lehmann and E. Callaway, editors, *Human Evoked Potentials: Applications and Problems*, pages 235–250, Plenum Press, New York, 1979.

[66] G. McCarthy and C. C. Wood. Scalp distributions of event-related potentials: An ambiguity associated with analysis of variance models. *Electroenceph. Clin. Neurophysiol.*, 62:203–208, 1985.

[67] J. W. H. Meijs and M. J. Peters. The EEG and MEG, using a model of eccentric spheres to describe the head. *IEEE Trans. Biomed. Eng.*, BME-34:913–920, 1987.

[68] B.A. Milner. Evaluation of auditory function by computer techniques. *Intl. Audiology*, 8:361–370, 1969.

[69] U. Mitzdorf. Properties of the evoked potential generators: Current source density analysis of visually evoked potentials in the cat cortex. *J. Neurosci.*, 33:33–59, 1987.

[70] U. Mitzdorf and W. Singer. Excitatory synaptic ensemble properties in the visual cortex of the macaque monkey: a current source density analysis of electrically evoked potentials. *J. Comp. Neur.*, 187:71–84, 1979.

[71] V.B. Mountcastle. An organization principle for cerebral function: The unit module and the distributed system. In F.O. Schmitt and F.G. Worder, editors, *The Neurosciences: Fourth Study Program*, pages 21–42, M.I.T. Press, Cambridge, 1979.

[72] B. B. Murdoch, Jr. and K. D. Walker. Modality effects in free recall. *Verbal Lrng. and Verbal Beh.*, 86:665–676, 1969.

[73] R. Näätänen. Neurophysiological basis of the echoic memory as suggested by event-Related potentials and magnetoencephalogram. In F. Klix and H. Hagendorf, editors, *Human Memory and Cognitive Capability*, pages 615–628, Elsevier/North-Holland, Amsterdam, 1986.

[74] R. Näätänen and T. Picton. The N1 wave of the human electric and magnetic response to sound. *Psychophysiology*, 24:375–425, 1987.

[75] U. Neisser. *Cognitive Psychology.* Appleton-Century-Crofts, New York, 1967.

[76] D.A. Nelson and F.M. Lassman. Effect of intersignal interval on the human auditory evoked response. *J. Acoust. Soc. Am.*, 44:1529–1532, 1963.

[77] Y. Okada. Discrimination of localized and distributed current dipole sources and localized single and multiple sources. In H. Weinberg, G. Stroink, and T. Katila, editors, *Biomagnetism: Applications & Theory*, pages 266–272, Pergamon Press, New York, 1985.

[78] Y. C. Okada. Recent developments on the physiological basis of magnetoencephalography (MEG). In S. J. Williamson, M. Hoke, G. Stroink, and M. Kotani, editors, *Advances in Biomagnetism*, pages 273–278, Plenum, New York, 1989.

[79] C. Pantev, M. Hoke, K. Lehnertz, B. Lütkenhöner, G. Anogianakis, and W. Wittkowski. Tonotopic organization of the human auditory cortex revealed by transient auditory evoked magnetic fields. *Electroenceph. Clin. Neurophysiol.*, 69:160–170, 1988.

[80] C. Pantev, M. Hoke, B. Lütkenhöner, and K. Lehnertz. Influence of stimulus intensity on the location of the equivalent current dipole in the human auditory cortex. In K. Atsumi, M. Kotani, S. Ueno, T. Katila, and S. J. Williamson, editors, *Biomagnetism '87*, pages 146–149, Tokyo Denki University Press, Tokyo, 1988.

[81] W. M. Paulus, H. Plendl, and S. Krafczyk. Spatial dissociation of early and later colour evoked components. *Electroenceph. Clin. Neurophysiol.*, 71:81–88, 1988.

[82] G. Pfurtscheller. Mapping of event related desynchronization and type of derivation. *Electroenceph. Clin. Neurophysiol.*, 70:190–193, 1988.

[83] G. Pfurtscheller and A. Aranibar. Event-related cortical desynchronization detected by power measurments of scalp EEG. *Electroeneceph. clin. Neurophysiol.*, 42:817–826, 1977.

[84] R. W. Picton, D. Woods, D. Stuss, and K. Campbell. Methodology and meaning of human evoked-potential scalp distribution studies. In D. A. Otto, editor, *Multidisciplinary Perspectives in Event-Related Brain Potential Research*, pages 515–522, U. S. Environmental Protection Agency, Washington, DC, 1978.

[85] R. W. Picton, D. L. Woods, and G. B. Proulx. Human auditory sustained potentials II. Stimulus relationships. *Electroenceph. Clin. Neurophysiol.*, 45:198–210, 1978.

[86] T. W. Picton and S. A. Hillyard. Human auditory evoked potentials. II. Effects of attention. *Electroenceph. clin. Neurophysiol.*, 36:191–199, 1974.

[87] T. W. Picton, D. L. Woods, and G. B. Proulx. Human auditory sustained potentials I. The nature of the response. *Electroenceph. Clin. Neurophysiol.*, 45:186–197, 1978.

[88] T.W. Picton, D. Woods, J. Baribeau-Braun, and T. Healey. Evoked potential auditometry. *J. Otolaryngology*, 6:90–119, 1977.

[89] R. Plonsey. Magnetic field resulting from action currents on cylindrical fibers. *Med. Biol. Eng. and Comp.*, 19:311–315, 1981.

[90] M. P. Regan and D. Regan. A frequency domain technique for using evoked magnetic fields to test multi-stage models of sensory processing. In S. J. Williamson, M. Hoke, G. Stroink, and M. Kotani, editors, *Advances in Biomagnetism*, pages 201–204, Plenum, New York, 1989.

[91] A.J. Rockel, R.W. Hiorns, and T.P.S. Powell. The basic uniformity in structure of the neocortex. *Brain*, 103:221–244, 1980.

[92] R. L. Rogers, A. C. Papanicolaou, S. Baumann, C. Saydjari, and H. M. Eisenberg. Nonstationary dynamics of sequential magnetic dipole source changes associated with N100 auditory evoked responses. In S. J. Williamson, M. Hoke, G. Stroink, and M. Kotani, editors, *Advances in Biomagnetism*, pages 105–108, Plenum, New York, 1989.

[93] G. L. Romani, I. Modena, and R. Leoni. Biomagnetism: Recent progress in Italy. In *Proc. Intl. Conf. on Appl. of Phys. to Medicine and Biology*, Trieste, Italy, March 1982.

[94] G. L. Romani, S. J. Williamson, and L. Kaufman. Tonotopic organization of the human auditory cortex. *Science*, 216:1339–1340, 1982.

[95] G. L. Romani, S. J. Williamson, L. Kaufman, and D. Brenner. Characterization of the human auditory cortex by the neuromagnetic method. *Exp. Brain Res.*, 47:381–393, 1982.

[96] B.J. Roth and J.P. Wikswo, Jr. The magnetic field of a single axon. *Biophys. J.*, 48:93–109, 1985.

[97] J. Rovamo, L. Hyvärinen, and R. Hari. Human vision without luminance-contrast system: selective recovery of the red-green colour-contrast system from acquired blindness. pages 457–466, 1982.

[98] M. Scherg, R. Hari, and M. Hämäläinen. Frequency-specific sources of the auditory N19-P30-P50 response detected by a multiple source analysis of evoked magnetic fields and potentials. In S. J. Williamson, M. Hoke, G. Stroink, and M. Kotani, editors, *Advances in Biomagnetism*, pages 97–100, Plenum, New York, 1989.

[99] M. Scherg, J. Vajsar, and T. W. Picton. A source analysis of the late human auditory evoked potentials. *J. Cognitive Neurosci.*, 1:336–355, 1989.

[100] M. Scherg and D. von Cramon. Evoked dipole source potentials of the human auditory cortex. *Electroenceph. Clin. Neurophysiol.*, 65:344–360, 1986.

[101] M. Scherg and D. von Cramon. A new interpretation of the generators BAEP waves I-V: Results of a spatio-temporal dipole model. *Electroenceph. Clin. Neurophysiol.*, 62:290–299, 1985.

[102] M. Scherg and D. von Cramon. Two bilateral sources of the late AEP as identified by a spatio-temporal dipole model. *Electroenceph. Clin. Neurophysiol.*, 62:32–44, 1985.

[103] V. L. Schwent and S. A. Hillyard. Evoked potential correlates of selective attention with multi-channel auditory inputs. *Electroenceph. Clin. Neurophysiol.*, 38:131–138, 1975.

[104] V. L. Schwent, S. A. Hillyard, and R. Galambos. Selective attention and the auditory vertex potential. I: Effects of stimulus delivery rate. *Electroenceph. Clin. Neurophysiol.*, 40:604–614, 1976.

[105] V. L. Schwent, S. A. Hillyard, and R. Galambos. Selective attention and the auditory vertex potential. II: Effects of signal intensity and masking noise. *Electroenceph. Clin. Neurophysiol.*, 40:615–622, 1976.

[106] R. Shapley. Visual sensitivity and parallel retinocortical channels. *Ann. Rev. Psychol.*, 41:635–658, 1990.

[107] G.M. Sheperd. *Neurobiology.* Oxford University Press, New York, 1988.

[108] S. Shipp and S. Zeki. Segregation of pathways leading from area V2 to areas V4 and V5 of macaque visual cortex. *Nature*, 315:322–325, 1985.

[109] J.J. Stockard, J.E. Stockard, and F.W. Sharbrough. Brainstem auditory evoked potentials in neurology: Methodology, interpretation, clinical application. In M.J. Aminoff, editor, *Electrodiagnosis in Clinical Neurology*, chapter 12, pages 370–413, Churchill Livingstone, New York, 1980.

[110] K. R. Swinney and J. P. Wikswo. A calculation of the magnetic field of a nerve action potential. *Biophys. J.*, 32:719–731, 1980.

[111] R.B.H. Tootell, M.S. Silverman, S.L. Hamilton, R.L. DeValois, and E. Switkes. Functional anatomy of macaque striate cortex. III. color. *J. Neurosci.*, 8:1569–1593, 1988.

[112] T. Tuomisto, R. Hari, T. Katila, T. Poutanen, and T. Varpula. Studies of auditory evoked magnetic and electric responses: Modality specificity and modelling. *Il Nuovo Cimento*, 2D:471–483, 1983.

[113] G. von Bonin. *J. Comp. Neurol.*, 69:181, 1938.

[114] G. von Bonin and P. Bailey. *The Neocortex of Macaca Mulatta.* University of Illinois Press, Urbana, IL, 1947.

[115] V. Vvedensky, R. Hari, R. Ilmoniemi, and K. Reinikainen. Physical basis of the generation of neuromagnetic fields. *Biophysics*, 30:154–158, 1985.

[116] J. P. Wikswo. Biomagnetic sources and their models. In S. J. Williamson, M. Hoke, G. Stroink, and M. Kotani, editors, *Advances in Biomagnetism*, pages 1–18, Plenum, New York, 1989.

[117] J. P. Wikswo, Jr. and J. P. Barach. An estimate of the steady magnetic field strength required to influence nerve conduction. *IEEE Trans. Biomed. Eng.*, BME-27:722–723, 1980.

[118] S. J. Williamson and L. Kaufman. Biomagnetism. *J. Magn. Magn. Mat.*, 22:129–201, 1981.

[119] S. J. Williamson and L. Kaufman. Neuromagnetism: A window on the brain. ELAN (Japan), Jan. 134-139; Feb. 148-151, 1988.

[120] S. J. Williamson and L. Kaufman. Theory of neuroelectric and neuromagnetic fields. In F. Grandori, H. Hoke, and G. L. Romani, editors, *Auditory Electric and Magnetic Fields*, pages 1–39, Karger, Basel, 1989.

[121] S. J. Williamson, J.-Z. Wang, and R. J. Ilmoniemi. Method for locating sources of human alpha activity. In S. J. Williamson, M. Hoke, G. Stroink, and M. Kotani, editors, *Advances in Biomagnetism*, pages 257–260, Plenum, New York, 1989.

[122] J. R. Wolpaw and J. K. Penry. A temporal component of the auditory evoked response. *Electroenceph. Clin. Neurophysiol.*, 39:609–620, 1975.

[123] C. C. Wood and J.R. Wolpaw. Scalp distribution of human auditory evoked potentials: II. Evidence for multiple sources and involvement of auditory cortex. *Electroenceph. Clin. Neurophysiol.*, 54:25–38, 1982.

[124] T. Yamamoto, S. J. Williamson, L. Kaufman, C. Nicholson, and R. Llinás. Magnetic localization of neuronal activity in the human brain. *Proc. Natl. Acad. Sci. USA*, 85:8732–8736, 1988.

[125] Z. Zeki. Colour vision and functional specialization in the visual cortex. *Discussions in Neuroscience*, VI:1–64, 1990.

[126] S.M. Zola-Morgan and L.R. Squire. The primate hippocampal formation: Evidence for a time-Limited role in memory storage. *Science*, 250:288–290, 1990.